CHAPTER 5: ASSESSMENT OF A SIMPLIFIED METHOD FOR PREDICTING PERFORMANCE

5.1 Overview

As discussed in Chapter 4, the key to performance of an improved ground zone supporting a bridge within a liquefiable soil deposit is the displacements, and in some cases the accelerations, that the treated zone and supported structure experience as a result of an earthquake. Predicting the displacements and accelerations, taking into account the phenomena and conditions influencing performance, is therefore a critical part in the design and evaluation process of ground improvement used for liquefaction mitigation.

Simplified methods for predicting the performance of an improved ground zone and supported structure would be desirable, from an ease of design standpoint, provided they are reliable. Therefore, the early stages of this research focused on the assessment of a simplified, uncoupled analytical approach. This approach utilized analyses and tools judged to be more common in geotechnical engineering practice than those used in more sophisticated, coupled analyses. The assessed method consisted of performing dynamic ground response, seepage, and pseudostatic stability and deformation analyses, as briefly described below.

Dynamic Ground Response Analysis: The dynamic response of the improved ground zone within the liquefiable soil deposit is predicted using a two-dimensional, equivalent linear dynamic response analysis with the program QUAD4M (Hudson et al., 1994). The program uses a finite element formulation. Analyses are performed using total unit weights and stresses such that pore water pressure development and migration are not included. Information obtained from the analyses include predicted shear stresses and strains and accelerations within the improved ground system. Based on the predicted shear stress information, the factor of safety against liquefaction is computed in all of the elements representing the improved and unimproved zones, from which excess pore water pressures are estimated. The accelerations predicted at nodal points are used to

estimate a seismic coefficient to be used, along with the predicted excess pore water pressures, in pseudostatic stability and deformation analyses of the improved zone.

Seepage Analyses: The migration of excess pore water pressures from the liquefied soil into the improved ground zone, during and after earthquake shaking, is estimated using either steady state or transient seepage analyses performed with the program MODFLOW (McDonald and Harbaugh, 1984). MODFLOW is based on a finite difference formulation and can be used to perform two- or three-dimensional (2-D or 3-D) analyses for groundwater flow in fully-saturated soil. The results from the seepage analyses of the treated zone are used to assess whether pore water pressures predicted from the dynamic response analyses need to be increased to account for migration before being used in stability and deformation analyses.

Stability Analyses: The overall stability of an improved ground and supported structure system within a liquefiable soil deposit is evaluated using pseudostatic stability analyses performed with the computer program UTEXAS3 (Wright, 1991). This program was developed for slope stability analyses using limit equilibrium procedures. The pore water pressures within the treated zone and pseudostatic seismic coefficient used in the stability calculations are estimated from the dynamic ground response and seepage analyses described above.

Deformation Analyses: Predictions of improved ground and supported structure movements are obtained from pseudostatic deformation analyses performed using the finite element method. These analyses are conducted with the finite element program SAGE (Morrison, 1995) developed for evaluating geotechnical problems involving static loading. As with the stability analyses, the pore water pressures and seismic coefficient are estimated from seepage and dynamic ground response analyses, respectively.

The intent of the sequence of uncoupled analyses described above is to provide a means of predicting the overall stability and deformation of the improved ground zone and supported structure, primarily taking into account the phenomena of ground motion amplification and pore

water pressure migration. The analytical methods were selected early in the research and prior to some studies by others (i.e. – Riemer et al., 1996) that looked at the potential of a few simplified methods for predicting improved ground performance.

The pseudostatic stability analyses proposed as part of this procedure are more rigorous than traditional pseudostatic analyses, where the seismic coefficient is typically approximated as some fraction of the gravitational acceleration or peak crest acceleration of an embankment. In addition, traditional pseudostatic stability analyses are used for soils that lose no more than 15 percent of their strength during shaking. Therefore, they do not attempt to account for changes in strength due to pore pressure generation resulting from shear and migration by estimating pore water pressures that develop from dynamic ground response and transient seepage analyses. The pseudostatic approach has generally only been applied to the stability of embankments or dams, and not the seismic stability of footings, as done herein. Likewise, pseudostatic deformation analyses have not been used in the past for estimating ground deformations.

An assessment of the capability of the selected uncoupled analyses (performed using the computer codes mentioned, or their equivalent) proposed for predicting treated ground performance is given below, along with the results of a series of test analyses used in the evaluation process.

5.2 Dynamic Ground Response

The feasibility of using results from QUAD4M to estimate excess pore water pressure development and accelerations within an improved ground zone was assessed by modeling a centrifuge test conducted by Adalier (1996). In this test fully-saturated dense and loose sand zones adjacent to each other were subjected to a simulated earthquake motion which induced complete liquefaction in the loose sand and caused high pore water pressures to develop in the dense sand.

5.2.1 Centrifuge Test Details

The centrifuge test set-up consisted of two vertical zones of fine sand (Nevada 120 sand) placed side by side in a rigid wall box at relative densities of 40 and 90 percent, as shown in Figure 5.1. The thickness and width (all dimensions and results are presented in prototype scale)

of each zone were 5 meters and 15 meters, respectively. The sand was saturated with a solution consisting of 60 percent glycerin and 40 percent water, giving the fluid a unit weight approximately 1.15 times that of water. This mixture of glycerin and water has a viscosity of approximately 10 times that of water alone and serves to counterbalance the increase in the soil hydraulic conductivity that results when the centrifuge model is subjected to high g forces. In the test the model was subjected to 10 cycles of a sinusoidal acceleration record having a frequency of 2 Hertz and amplitude of 0.19g. The response of the model during shaking was monitored using accelerometers, pore water pressure transducers, and linear variable displacement transducers (for monitoring settlement) at the locations shown in Figure 5.1. In addition, the lateral displacement at the boundary between the loose and dense sand was monitored using three spaghetti noodles placed at the boundary and 0.5 meters on each side of the boundary.

5.2.2 QUAD4M Modeling and Results

The dynamic response of the loose-dense sand model was analyzed using the finite element grids shown in Figures 5.2 and 5.3, respectively, with the coarser grid being used in an analysis unless otherwise noted. All analyses were conducted using prototype scale dimensions and the properties given in Table 5.1 for the loose and dense sand zones. Peak accelerations were obtained at all nodal points and peak shear stresses and shear strains in all elements, as well as time histories of accelerations and stresses at select locations.

Maximum shear moduli used for the elements representing the dense sand in the QUAD4M analyses were computed using the formulation by Seed and Idriss (1970):

$$G_{max} = 1000\ K_{2max}\ (\sigma'_m)^{0.5} \qquad (5.1)$$

where:

G_{max} is the maximum shear modulus in pounds per square foot, psf (later converted to kilopascals, kPa),

K_{2max} is the shear modulus number for the soil, and

σ'_m is the mean effective confining stress of the soil in psf.

Reduced shear moduli for these elements, based on the shear strain level during shaking, were obtained using the shear modulus degradation values for sand recommended by Idriss (1990), as given in Table 5.2. The shear moduli for the elements in the loose sand zone were determined in the same fashion as the dense sand for the initial analyses. In all analyses the damping ratio used for the dense sand was based on recommended values by Idriss (1990), as given in Table 5.2. This same damping ratio curve was also used for the loose sand in the initial analyses.

An estimate of the excess pore water pressure that develops in each element due to the induced shear strain during shaking was obtained by first computing the factor of safety against liquefaction for each element. In order to estimate the factor of safety against liquefaction, the cyclic stress ratio (CSR) in each element was computed using the peak shear stresses (shear stress amplitude was relatively constant in an element throughout the simulated shaking) and the estimated effective overburden pressure. The cyclic resistance ratio (CRR) in the dense and loose sands was obtained by estimating an equivalent corrected standard penetration resistance, $(N_1)_{60}$, for the sands and using the liquefaction resistance chart originally developed by Seed and Idriss (1970) and updated by NCEER (1997). A magnitude correction factor of 1.4 was applied to the CRR based on the equivalent earthquake magnitude for the number of cycles of motion applied in the test. Two values for the factor of safety against liquefaction were computed by dividing CRR by CSR: the first without the CRR corrected using the overburden correction factor, K_σ, and the second with the CRR corrected. The excess pore water pressure ratio, r_u, that develops in each element was then estimated using the correlation between the factor of safety against liquefaction and r_u for sand proposed by Marcuson and Hynes (1989), and presented by Seed and Harder (1990), as shown in Figure 5.4. Excess pore pressure ratio is defined as the magnitude of pore pressure that develops over and above the initial static pore water pressure divided by the initial effective vertical stress.

As expected the QUAD4M analyses generally indicated complete liquefaction ($r_u = 1.0$) in the loose sand zone, while the dense sand zone was predicted to develop some high excess pore water pressures, but generally not enough to cause complete liquefaction. When the shear modulus for the loose sand zone was based on a maximum shear modulus computed using a shear modulus number, K_{2max} (Seed and Idriss, 1970), of 41 and the modulus degradation curves recommended by Idriss (1990), the predicted excess pore water pressure ratios in the dense sand were lower than measured. For this reason, analyses were performed using reduced shear moduli

for the loose sand to represent it in a liquefied state, with the modulus and damping ratio of the loose sand being held constant in any given analysis (no modulus degradation due to shear strain during shaking). The idea behind this approach was that lowering the loose zone modulus would result in larger predicted deformations and excess pore water presssures in the dense zone that agreed more closely with the measured values.

Figures 5.5 to 5.14 present results from two sets of analyses in which reduced shear moduli were used for the loose zone. In one set of analyses the vertical boundaries at the sides of the grid were fixed in the horizontal (x) direction (i.e. – constrained to following the input x-acceleration record) and free in the vertical (y) direction (i.e. – vertical movement not restricted) and in the other the sides were free in the x-direction (i.e. – horizontal movement not constrained) and fixed in the y-direction (i.e. – no vertical movement allowed). The bottom boundary was fixed in both directions in all analyses (i.e. – constrained to following the input x-acceleration record and restricted from movement in the y-direction) and a constant damping ratio of 25 percent was assumed for the liquefiable, loose sand for the constant, reduced modulus cases. The results presented in these plots are for the dense zone and include the variation of the average liquefaction safety factor for all elements in the zone, average of the peak shear strains (shear strain amplitude was relatively constant in an element during simulated shaking) for the zone, excess pore water pressure ratio r_u in five select elements (labeled CP2 and CP7 through CP10 in Figure 5.2), and peak x-accelerations at three select nodal points (labeled CA4, CA5. and CA7 in Figure 5.2). These data are plotted against the first natural period of the entire system computed by QUAD4M, which is dependent in part on the shear modulus assumed for the loose sand zone in each analysis. The assumed loose zone modulus associated with each data point is noted adjacent to the point in the first plot of a group.

As seen from Figures 5.5 to 5.14, when the first natural period of the loose-dense system is close to input motion period of 0.5 seconds (for input frequency of 2 Hz) the predicted average factor of safety against liquefaction for the dense zone is the lowest (Figure 5.5), average shear strain is the highest (Figure 5.6), r_u values in the selected elements are the highest (Figures 5.7 to 5.11), and peak x-accelerations at selected nodes are the highest (Figures 5.12 to 5.14). The plots in Figures 5.7 to 5.10 and 5.12 to 5.14 indicate that the predicted dense zone response was closest to the measured one when the assumed loose zone modulus gave a first natural period for the entire system close to the input motion period. This observation holds for both types of side

boundary conditions used. The observed pattern in the results would be expected because it suggests that the peak response of the dense zone occurs when the loose-dense sand system is close to resonance during shaking.

It is interesting to note that the side boundary conditions with y fixed and x free gives results closer to those measured in the centrifuge test than with y free and x fixed, even though the latter seem more appropriate for representing the behavior occurring in a centrifuge model box having rigid walls. This may indicate some discrepancy in the actual behavior occurring at the sides of the rigid box compared to what might be assumed. In particular, the progressive softening of the loose sand during the shaking may have permitted more lateral movement of the loose-dense system relative to the box during the test than allowed in QUAD4M using the side boundaries fixed in the x-direction. For analysis purposes the y fixed and x free side boundary condition in the QUAD4M analyses appears to model the actual behavior better. Therefore it was used in the other comparative analyses performed, as described later in this section.

In the plots of factor of safety against liquefaction for the dense zone (Figure 5.5) and the excess pore pressure ratio for select elements (Figures 5.7 through 5.11) versus the first natural period of the system, there are reversals in the predicted trends at a period of about 2 seconds and above. These discontinuities are due to the mesh shown in Figure 5.2 being too coarse for the low shear modulus of the loose zone per the criteria recommended by Kuhlemeyer and Lysmer (1973) for maintaining accuracy in numerical modeling of dynamic response. When the finer mesh shown in Figure 5.3 is used for the analysis where the loose zone shear modulus is 65 kPa, the discontinuities are removed, as shown in Figures 5.15 and 5.16.

Another set of QUAD4M analyses was performed to study the effect of the assumed damping ratio for the liquefiable, loose sand on the predicted results. Constant damping ratios of 10 percent and 40 percent were used for the loose sand along with the same values of constant, reduced shear modulus. These damping ratios were selected as upper and lower bounds for the liquefied, loose sand. The shear modulus used in the analyses for the dense sand was computed using the maximum shear modulus and modulus degradation values in Table 5.2 and the damping ratio was obtained from the same table, as discussed previously.

Figures 5.17 through 5.20 present results for the dense zone for the average liquefaction safety factor, average shear strain, r_u in element CP9, and horizontal acceleration at node CA7 for the damping ratios of 10 and 40 percent, along with the 25 percent ratio. The plots in Figures

5.17 and 5.19 indicate a 25 percent damping ratio gives a lower liquefaction safety factor and better agreement between predicted and measured r_u values at select elements than the other damping ratios. The average shear strain and peak x-accelerations do not appear to be as sensitive to changes in the damping ratio, as evident from the plots in Figures 5.18 and 5.20. The shear strain, r_u, and peak x-acceleration plots still indicate that a peak response is obtained when the system period is close to the input motion period, regardless of whether the damping ratio is 10, 25, or 40 percent.

Even using a damping ratio of 25 percent and side boundaries fixed in the y-direction, the predicted r_u values and peak horizontal accelerations for the dense zone were lower than measured. However, these analyses were conducted assuming the pore fluid in the centrifuge test was water having a unit weight of 9.8 kilonewtons per cubic meter (kN/m^3). The actual pore fluid was a mixture of 60 percent glycerin and 40 percent water having a reported unit weight of 1.15 times that of water (Adalier, 1996) and a viscosity approximately 10 times that of water. A set of QUAD4M analyses was performed using a reduction in the maximum shear modulus for the dense sand resulting from the lower effective stress associated with the use of the glycerin-water mixture. In these analyses a damping ratio of 25 percent was used for the loose, liquefied sand having a reduced modulus and side boundaries were fixed in the y-direction. The shear modulus and damping ratio used for the dense sand were the same as previously described. Figures 5.21 to 5.24 present the results for the dense zone for the average liquefaction safety factor, average shear strain, r_u in elements CP9, and x-acceleration at node CA7 obtained for the glycerin-water case, along with the "pure" water results. As seen from these plots the glycerin-water case has a lower predicted factor of safety and higher average shear strain, element r_u, and peak x-acceleration values. The use of soil properties associated with the higher fluid density brought the predicted response for the dense zone closer to the measured.

To further confirm if the occurrence of the peak response of a loose-dense system predicted by QUAD4M was a function of soil properties producing a system period close to the input motion period, another set of analyses was performed using an input motion having a frequency of 0.5 Hz and a period of 2 seconds. The results of these analyses are presented in Figures 5.25 to 5.28, along with the results for the input motion having a 0.5 second period. In both sets of analyses the side boundaries were fixed in the y-direction, damping ratio for the loose sand having a reduced modulus was fixed at 25 percent, and a pore fluid density for "pure"

water was used. As seen in Figures 5.25, 5.26, and 5.28, the loose zone shear modulus producing the most critical response for the average liquefaction safety factor, average shear strain, and peak x-accelerations for the input motion having a 2 second period is the one producing a system period close to 2 seconds. The occurrence of a peak pore water pressure response at a system period of 2 seconds is not clearly evident in Figure 5.27.

All of the results from the QUAD4M analyses performed indicate that a peak response for a loose-dense system is tied to the stiffnesses of the loose and dense zones degrading to the point where the first natural period of the system approaches the predominant input motion period. Using the maximum shear modulus for the liquefiable, loose sand along with the typical shear modulus degradation curve (i.e. – Idriss, 1990) can result in missing the peak response of the system. Likewise, using a greatly reduced shear modulus for the loose soil may not result in the peak response being obtained. It is likely the peak response will only be predicted when the shear modulus of the liquefiable, loose sand is reduced to the point where it, along with the degraded dense zone modulus, result in a first natural period for the system close to the input motion period.

5.2.3 Implications for Use of QUAD4M

The use of QUAD4M to predict the centrifuge test by Adalier (1996) has indicated a shortcoming of using the program, and the equivalent linear method, in predicting the dynamic behavior of an improved ground system, such as a densified zone within a liquefiable soil deposit. The results indicate that unless a degraded shear modulus is used for the liquefiable soil such that it, along with the improved zone modulus, produces a first natural period for the system close to the predominant input motion period, the peak response for the improved ground is likely to be missed. Using extremely low values for the liquefiable zone stiffness generally will not produce conservative predictions of response because this can result in a system period which is higher than the predominant periods of the input motion. It appears that obtaining the peak response of a system using QUAD4M would involve a trial and error procedure where the stiffness of the liquefiable soil is reduced progressively until the peak response is obtained. This approach is fairly straightforward, but time consuming, for a simple system where the input motion has only one period associated with it. However, in a real system that is more complicated and where the input motion includes a range of frequencies, the approach is more difficult. In addition, in a real system the properties of the unimproved and improved zones will

change during shaking which may alter the frequency content of the input motion as it passes upward through the system. The QUAD4M approach also does not account for the changes in the stiffness of the improved zone during shaking due to pore water pressure changes within the zone, which also affect the dynamic response. In conclusion, this approach for predicting the dynamic response of an improved ground system is difficult and may not be successful for estimating the peak pore water pressures and accelerations that develop within the improved zone for use in other analyses that are part of the uncoupled analysis procedure.

5.3 Seepage Analyses

As discussed in Chapter 4, Section 4.3.1, the migration of excess pore water pressures into an improved ground zone within a liquefiable soil deposit during and after earthquake shaking has the potential for increasing the risk of instability and excessive deformations of the zone and supported structure. This phenomenon is a particular concern for improved zones created by densification because densification of a cohesionless soil will not likely reduce the soil hydraulic conductivity significantly. The groundwater seepage program MODFLOW was evaluated as a means for predicting increases in excess pore water pressures within densified zones due to migration. This program was also used to further study the phenomenon of migration. These analyses were conducted by graduate student Jennifer Schaeffer, and are explained in greater detail in her Master's report entitled "Excess Pore Water Pressure Migration and Dissipation in Densified Sand Zones During and After Earthquakes" (Schaeffer, 1998).

5.3.1 Analytical Approach

For the purposes of evaluating pore water pressure migration into a densified zone using a groundwater modeling program, the phenomenon was divided into two distinct phases. The first phase consisted of the pore water pressure migration occurring during earthquake shaking (referred to as the "migration" phase); the second phase involved pore pressure dissipation after strong shaking stopped (referred to as the "dissipation" phase). Analyses performed using MODFLOW show that both the migration and dissipation phases can have significant effects on the predicted pore water pressures and should both be evaluated as a combined process (i.e. - combined migration and dissipation analyses)

In the migration phase the time at which liquefaction occurs during earthquake shaking is estimated. The migration that occurs during the remainder of strong shaking is then evaluated using a transient seepage analysis. In this analysis, a pore water pressure distribution for the liquefied soil (calculated using the total unit weight of the liquefied soil) is applied at the boundary of the dense zone and pore pressures in the zone are initially set to values compatible with the shear strains. A schematic of boundary conditions for a 2-D analysis using this approach is shown in Figure 5.29(a), applying symmetry about the dense zone centerline. From this analysis, time histories of predicted pore water pressures at various points in the dense zone during strong shaking due to migration can be estimated, as well as the predicted values at the end of shaking.

The dissipation phase involves estimating the change in pore water pressures that occur within the dense and loose zones over time after strong shaking stops. In this analysis both zones must be modeled, as shown in Figure 5.29(b) for a 2-D case. The pore water pressures in the dense zone at the beginning of the analysis are set to the values obtained at the end of the migration phase. A fully-liquefied, loose zone will have an excess pore water pressure ratio, r_u, of 1.0 at the start of the dissipation phase. Appropriate drainage boundary conditions are set in the model and the transient analysis run until significant dissipation has occurred.

An example of a pore water pressure plot for a point in a dense zone obtained using the combined migration and dissipation analysis approach is shown in Figure 5.30. This particular plot is for Point A in the dense zone shown in Figure 5.29, with the properties and dimensions of the loose and dense zones used in the analysis also given in that figure. The pore water pressure is expressed in terms of the excess pore water pressure ratio, r_u. In addition, the r_u value estimated at that point using a steady state seepage analysis for the migration phase is indicated on the plot. The steady state value typically provides an estimate of the upper bound r_u that can develop during or after the earthquake for the given boundary conditions, provided the initial r_u in the dense zone due to shear strain is not excessively large.

5.3.2 Verification of Method

The proposed migration-dissipation analysis method of evaluating pore water pressures in densified zones during and after shaking using MODFLOW was tested by simulating a shaking table test performed by Iai et al. (1988). The shaking table test involved adjacent loose and dense sand zones, as shown in Figure 5.31, subjected to three successive steps of shaking

consisting of 20 cycles of a 10 Hertz sinusoidal input acceleration having amplitudes of 0.047g, 0.12g, and 0.21g, respectively. Pore water pressures and accelerations in the loose and dense sands were measured with a series of pore water pressure transducers and accelerometers. Excess pore water pressures were allowed to dissipate from one step of shaking before proceeding to the next.

In the series of tests performed, liquefaction of the loose sand was not observed during shaking for the input acceleration of 0.047g, but was observed for the higher accelerations of 0.12g and 0.21g. For the 0.12g input, liquefaction of the loose zone was observed at the end of the two-second-long shaking and for the 0.21g input it occurred at about 0.6 sec into shaking.

MODFLOW analyses were performed for the last shaking event having an amplitude of 0.21g to compare pore water pressures in the dense zone predicted using the migration-dissipation analysis with the values actually measured. This comparison was made in the row of ten pore pressure transducers shown in Figure 5.31. The boundary conditions used in the migration and dissipation phases of the evaluation are shown in Figure 5.32. Hydraulic conductivity, k, and volume compressibility, m_v, values for the loose and dense sands initially used in the analyses were those given by Iai et al. (1988) and are summarized in Table 5.3.

Using the soil property values given by Iai et al. (1988) resulted in MODFLOW predictions of pore water pressures in the dense zone at the end of the migration phase (i.e. – end of strong shaking) being lower than those measured in the row of ten pore pressure transducers. Good agreement was obtained when the dense zone m_v used in MODFLOW was taken as 1/20 of the value presented in Table 5.3. For the dissipation phase of the analysis, reasonable agreement (i.e. – predicted values were 75 to 100 percent of measured values) between predicted and measured pore water pressures in the loose and dense zones were obtained by using 1/10 and 1.5 times the m_v values given in Table 5.3 for the dense and loose sands, respectively.

Although the reductions in m_v used for the dense zone to obtain reasonable agreement between predicted and measured results seem potentially excessive, Hilf (1991) indicates that sand compressibility for virgin loading may be 8 to 16 times the value for reloading. The reductions in dense zone compressibility therefore seem consistent with this information, provided the compressibility for the dense zone given by Iai et al. (1988) is a virgin compression value. Iai (1996), in a personal communication, stated the soil compressibilities given in Table 5.3 were reasonable for the sands during the test and no significant reduction in the values were

required for analysis purposes (i.e. – Iai at al. used one-half of the m_v values in Table 5.3 for their numerical modeling of the problem). He indicated the difference between predicted and measured pore water pressures was more likely to be a function of other factors, such as changes in the loose and dense zone hydraulic conductivities and K_o conditions during the test.

Given the changes in the compressibility and hydraulic conductivity of the dense and loose sands that likely occurred during and after shaking in the shaking table test, selecting single representative values for these properties to use in an analysis was difficult. This complication probably contributed to some of the discrepancies between predicted and measured values, along with the fact the MODFLOW analyses did not include any pore pressure generation within the dense zone due to the shear strain that occurred in the zone during shaking. Despite these shortcomings, the results of the MODFLOW simulations seem to indicate that reasonable trends in pore water pressure behavior during and after shaking can be obtained by analyzing the problem using the combined migration and dissipation phase approach.

5.3.3 Observations Regarding Migration and Dissipation

A series of transient seepage analyses were performed with the program MODFLOW to study pore water pressure migration and dissipation in a densified zone surrounded by liquefied soil. The purpose of these analyses was to investigate:

- Differences in pore water pressure development at different points within the densified zone,
- Effect of the initial pore water pressure in the densified zone at the start of migration on the pressures developed during migration and dissipation, and
- Difference in predicted pore water pressures for 2-dimensional (2-D) as opposed to 3-dimensional (3-D) analyses.

The study was conducted using the densified zone configuration shown in Figure 5.33. For the 2-D analysis the configuration shown in the section view was assumed to have an infinite length, whereas in the 3-D case the zone was given a limited length of 28-m, as shown in the plan view. Due to the symmetry existing in the 2-D and 3-D problems, only one half and one quarter of the treated zone was analyzed in the 2-D and 3-D problems, as illustrated in Figures

5.33(a) and 5.33(b). Impermeable boundaries were placed along the lines/planes of symmetry. The assumed properties for the loose and dense sands are presented in Table 5.4.

Figure 5.34 presents curves of predicted excess pore water pressure ratio at points 1 and 2 in the dense zone shown in Figure 5.33 obtained from 2-D and 3-D transient seepage analyses. In the analysis used to generate these curves, the soil profile was assumed to be subjected to 40 seconds of strong motion (i.e. – equivalent to a magnitude 7.5 earthquake), with liquefaction occurring in the loose sand after the first 10 seconds. Therefore the resulting migration period was 30 seconds, as indicated in Figure 5.34. The r_u in the dense zone at the start of the 30 second migration period was assumed to be 0.1. The straight lines shown in Figure 5.34 indicate the upper bound r_u values expected at the points for the 2-D and 3-D cases, as obtained from 2-D and 3-D steady state seepage analyses.

From the results presented in Figure 5.34, along with results from similar 2-D analyses where the initial r_u in the dense zone was assumed to be 0.3 instead of 0.1, the following observations can be made (Schaeffer, 1998):

- "The magnitude of the peak r_u within the densified block is a function of position in the densified block and initial r_u value. The closer a point is to the liquefied boundary, as measured perpendicular to the boundary, the greater the peak r_u value. The greater the initial r_u value, the greater the peak r_u value attained at any point in the densified block.
- The time to reach the peak r_u within the densified block is a function of position in the densified block and the initial r_u value. The closer a point is to the liquefied boundary, as measured perpendicular to the boundary, the faster the peak r_u values are attained. The greater the initial r_u value, the faster the peak r_u values are attained.
- In general, the 3-D analyses yield higher pore water pressures than the 2-D analyses. The 3-D condition has the most influence on points farthest from the liquefaction boundaries."

The data in Figure 5.34(a) for Point 1 indicate that the peak pore water pressure at a point in a densified zone may be reached after shaking has stopped and dissipation is in progress. The 2-D seepage analyses also confirmed that high excess pore pressure ratios on the order of 0.5 and

higher are developed at the boundary of the dense zone, as suggested by Iai et al. (1988) and Akiyoshi at al. (1994).

5.3.4 Implications for Design and Analysis

The results of the MODFLOW analyses performed suggest it can be a useful tool for understanding the migration and dissipation of excess pore water pressures that occur between liquefied and densified zones. Analyzing the problem as a combination of migration and dissipation phases which account for seepage that occurs during and after the earthquake, respectively, appears to provide a reasonable approximation of the actual behavior.

From the verification and parametric studies performed using MODFLOW it is apparent that the magnitude of pore water pressure that develops within a densified zone due to migration and dissipation is influenced by a number of factors. In particular it is dependent on the duration of the earthquake, relative hydraulic conductivities and compressibilities of the treated and untreated soil, and the drainage boundary conditions. For some conditions, particularly when the soil hydraulic conductivity is high, it's compressibility is low, and the earthquake duration is long, evaluation of the "migration" stage using a steady state seepage analysis is adequate for predicting upper bound pore water pressures in the densified zone.

It is important to note that the magnitude of the predicted pore water pressures is particularly sensitive to the soil hydraulic conductivity (k) and volume compressibility (m_v). Since these properties continually change during the liquefaction, migration, and dissipation processes, selecting single representative values for these properties for each soil type is difficult and places a limitation on the method. This limitation generally does not exist as much in coupled effective stress analyses because soil properties, such as compressibility, are usually updated as the simulated shaking and associated pore water pressure development are modeled.

Despite the shortcomings of the uncoupled seepage analyses for evaluating migration and dissipation of pore water pressures, they are still useful for quantifying the effect of using a 2-dimensional representation of a 3-dimensional problem. This effect could particularly be significant for treated zones that are approximately equi-dimensional in plan. The 2-D and 3-D uncoupled seepage analyses could potentially be used to develop a factor for incrementing pore water pressures in 2-D coupled analyses being used to predict performance of a 3-D improved ground zone. These incremented pressures would likely be more representative of the pore water pressures developing in the true 3-D problem, and produce a more realistic prediction of

performance for design. Likewise, if the engineer is limited to uncoupled analyses for predicting improved ground performance, then seepage analyses with MODFLOW can provide a rough estimate of the additional pore water pressures that could develop in the improved ground zone due to migration and dissipation.

5.4 Stability and Deformation Analyses

Prediction of improved ground performance ultimately requires assessing whether gross failure of the treated ground and supported structure will occur, and if not, whether the expected ground and structure movements will be compatible with the performance requirements specified for the structure. Potential methods for assessing the stability and deformations of such a treated ground and structure system, as part of an uncoupled analytical approach, can include pseudostatic stability and deformation analyses. In the pseudostatic analyses that are part of the uncoupled analytical approach proposed herein, a seismic coefficient is incorporated to approximate inertial loads induced in the ground by the design earthquake. This coefficient is estimated in the proposed approach from predicted ground accelerations obtained from dynamic ground response analyses, such as those performed with the program QUAD4M. Loads exerted by the structure on the foundation for the design earthquake are also included in the analyses. Excess pore water pressures that develop in an improved zone due to induced shear strain and pore pressure migration are estimated for inclusion in the analyses, as previously discussed in Sections 5.2.2 and 5.3.

To investigate the feasibility of using pseudostatic stability and deformation analyses for predicting improved ground behavior, a parametric study was performed using a test problem to evaluate the reasonableness of the results obtained. Based on the results, conclusions are drawn regarding the potential of the proposed pseudostatic approach for predicting treated ground performance.

5.4.1 Test Problem

A number of seismic design example problems developed for the Federal Highway Administration (Buckle and Friedland, 1995; Mast et al., 1996) were reviewed as potential test problems for evaluating the pseudostatic approach of predicting stability and deformations. The

test problem used in the parametric study was developed by modifying a highway bridge seismic retrofit example given in Appendix D (Worked Example Problem No. 2) of the "Seismic Retrofitting Manual for Highway Bridges" by Buckle and Friedland (1995). The example provided a framework for the bridge pier and span configurations used in the test problem, as well as the pier loads.

A schematic of the bridge used for the test problem is presented in Figure 5.35. It consists of four simply-supported spans, each having a length of 21 meters. The approaches are 6-meter-high embankments constructed of dense, well-graded gravelly sand supporting stub abutments founded on spread footings, as illustrated in Figure 5.36. Between the abutments the bridge spans are supported by three piers that are five meters high. Each pier consists of two four-meter-high columns with a one-meter-high cap across their tops and supported below on a four-meter-wide by eight-meter-long by one-meter-thick spread footing, as illustrated in Figure 5.37. The entire bridge is founded on top of a three-meter-thick medium dense sand layer over an eight-meter-thick loose sand layer underlain by stronger deposits. Both sand deposits have a fine to medium gradation and are liquefiable. The groundwater level at the site is at the natural ground surface, which is the top of the medium dense sand layer.

Individual column loads for the bridge piers and total loads for each stub abutment, based on AASHTO (1996) Service Load Group I, are summarized in Tables 5.5 and 5.6, respectively. These loads do not include any seismic component, and consist primarily of dead and working live loads. Loads at the base of individual pier columns for the seismic case, based on AASHTO Service Load Group VII, are presented in Table 5.7 for a design seismic coefficient of approximately 0.15 to 0.2. These loads consist mostly of the dead loads and the inertial forces induced on the dead loads by the design earthquake. The seismic loads in Table 5.7 are for the case where the design earthquake is assumed to act primarily in the same direction as the longitudinal axis of the bridge, which was the only case studied. Table 5.8 presents the magnitude and location of equivalent forces or stresses at the base of the footing that were used to replace the column loads in the two dimensional stability and deformation analyses performed.

The footing sizes for both the piers and stub abutment were found to be adequate to support the Group I Loads in Tables 5.5 and 5.6. For the earthquake loading case, liquefaction of the loose and medium dense sand layers was expected, resulting in inadequate support and excessive movements of the piers and abutments.

One possible method for reducing the occurrence of liquefaction-induced damage to the test problem bridge would be to improve the liquefiable sands beneath and around individual piers and abutments, creating treated zones of limited size for support of these components, as shown in Figures 5.38 and 5.39. The potential of using pseudostatic stability and deformation analyses for predicting the performance of improved ground was investigated using one of the test problem bridge piers supported on a densified zone having the same basic configuration shown in Figure 5.38. The evaluation was limited to earthquake-induced loading along the longitudinal axis of the bridge, and the analyses performed were two-dimensional using the section shown in Figure 5.38(a).

In performing the assessment of the pseudostatic analysis approach using the pier and densified zone problem, several conditions were varied to study the effect on the analysis results. These conditions included the densified soil properties, width of the treatment zone, seismic forces acting on the soil mass, and excess pore water pressures within the treated zone.

For the purposes of evaluating the pseudostatic methods, the pier and densified block were evaluated without considering the influence of adjacent piers or abutments. Therefore, the width of the treated zone at the pier was not limited by the distance to an adjacent pier or abutment and the potential for overlapping of treated zones. The improved zone and pier were considered to be isolated and only surrounded by liquefiable soil to restrict the changes in performance of the system to the effects of the conditions assumed for the treated zone. In the design of a comprehensive ground improvement scheme for the entire bridge, the presence of the adjacent piers and abutments would need to be taken into consideration.

The analyses and parametric study used to evaluate the potential of pseudostatic stability and deformation analyses for predicting improved ground performance are discussed below.

5.4.2 Pseudostatic Stability Analyses

The stability of the bridge pier supported on a densified ground zone was evaluated using pseudostatic analyses performed with the computer program UTEXAS3 (Wright, 1991). A schematic of the improved ground and loading configuration analyzed is given in Figure 5.40. The bearing pressures shown for the pier footing in the figure are those presented in Table 5.8, along with additional pressures to account for the footing weight. In performing the analyses, only the portion of the densified zone generally considered to be stable (area ABCD typically having excess pore water pressure ratios less than 0.5, as observed from shaking table tests and

numerical modeling analyses by Iai et al. (1988) and Akiyoshi et al. (1994) of densified zones without a surface load), was included in the stability evaluation. A portion of the densified zone along the boundary with the liquefiable soil, where the excess pore water pressure ratio has been found to be greater than 0.5 (area CDE in Figure 5.40 per Iai et al. and Akiyoshi et al.), was treated as liquefied in accordance with comments by Iai et al. (1988) regarding the strength in this area. Along the edge of the stable portion (lines AB and CD) the pressure exerted by the liquefied soil mass was applied as a distributed load. In many of the stability analyses performed, the sloping surface and liquefied soil pressure was only included on the side of the improved zone located in the direction of the seismic force to simplify the analysis set-up. A limited number of cases where both sloping sides of the densified zones were included, as shown in Figure 5.40, gave the same results as the corresponding cases where only one sloping side was used.

The stability of the pier footing shown in Figure 5.40 was evaluated for a number of different conditions. These conditions included variations in the densified soil properties, width of the treated zone beyond the edge of the footing (represented by a width to depth of treatment ratio), magnitude of the seismic coefficient controlling horizontal forces on the soil mass, and excess pore pressure developed within the zone during shaking. A summary of the different cases analyzed is given in Table 5.9. All analyses were performed using total unit weights and pore water pressures to eliminate input of seepage forces. The results of the analyses are discussed below along with results from the pseudostatic deformation analyses.

5.4.3 Pseudostatic Deformation Analyses

Potential movements of the densified ground zone and supported pier footing, when subjected to the design earthquake and liquefaction of surrounding soils, were predicted using pseudostatic deformation analyses performed with the finite element program SAGE (Morrison, 1996). The finite element mesh used in some of these analyses is shown in Figure 5.41, for the case where the treatment width beyond the edge of the footing was equal to the treatment depth of 10 meters below the footing. For simplicity only the densified zone and footing were modeled in the analyses, with the intent of providing a rough approximation of the deformation behavior for evaluation of the pseudostatic method. No interface elements were used between the footing and adjacent densified soil elements.

Each pseudostatic analysis was performed in a succession of steps. In the pre-earthquake steps, the static footing load was applied as a distributed load acting on the mesh for the entire densified zone, as shown in Figure 5.41(a), to establish the initial stress state. The earthquake loading steps consisted of removing the elements in the unstable portion of the densified zone to the right and left of lines AB and CD, respectively, and replacing them with a surface pressure acting along those lines, as shown in Figure 5.41(b). In addition a seismic coefficient was input to simulate the inertial effect of the earthquake on the soil mass, and the footing load was adjusted to incorporate the seismic components from the structure in accordance with the values given in Table 5.8. The deformations and stresses within the densified soil mass were then calculated in SAGE for this earthquake-induced liquefaction condition.

In the SAGE analyses performed, the Duncan and Chang (1970) hyperbolic model was used to represent the stress-strain behavior of the soil during the pre-earthquake and earthquake loading stages. Hyperbolic model parameters and strength properties assigned to the densified zone are given in Table 5.10. Since the soil stress-strain behavior and strength in the models used were governed by effective stresses, buoyant unit weights were input for the soil because a means of directly incorporating pore water pressures was not available in the version of SAGE used. In cases where the effects of excess pore water pressures in the densified zone were modeled, the buoyant unit weight of the densified soil was appropriately adjusted to account for the effect of the excess pressure. Seismic coefficients were factored up to account for the fact buoyant unit weights were being used in the analysis, but the seismic force acts on the total weight of the soil. Seepage forces were not included because they needed to be input on a node by node basis and accurately computing the distribution of these forces among the nodes was difficult. The results obtained without seepage forces should be somewhat conservative.

A series of pseudostatic deformation analyses were performed to investigate the effects of densified soil zone properties, width of the treated zone beyond the edge of the footing (represented by a width to depth of treatment ratio), magnitude of the seismic coefficient, and excess pore pressure developed within the zone during shaking on the predicted footing movements. The different cases evaluated are given in Table 5.10 and the results are presented below. This series of analyses paralleled the pseudostatic stability analyses performed and summarized in Table 5.9.

5.4.4 Results of Analyses

Figure 5.42 shows an example of a critical failure surface obtained for one of the pseudostatic stability analyses performed for the pier footing. The calculated factor of safety for this circular arc surface is 1.06 using Spencer's method. The critical failure surface for many of the other cases analyzed were similar to the one in Figure 5.42. Most of them started at the interior edge of the heavily loaded zone (156 kPa bearing pressure) at the base of the footing. The critical failure surface was not constrained to pass through the edge of the footing in these analyses to account for a potential tilting failure. This is more conservative (i.e. – results in a lower estimated factor of safety) than constraining the surface to pass through the edge of the footing.

Results from the pseudostatic deformation analyses indicate the pier footing is pushed downward and laterally in the direction of seismic loading from the structure and the seismic force acting on the soil mass, as shown in Figure 5.43. The maximum downward movement of the pier footing occurs at the edge where the large bearing pressure acts. Uplift is predicted at the opposite edge of the footing. The mesh representing the stable portion of the densified zone deforms laterally in the direction of the seismic forces. Vertical deformation of the mesh tends to follow the vertical displacement of the footing, with the downwardly displaced portion of the footing resulting in downward compression of the mesh beneath it and the upwardly displaced portion resulting in upward extension of the mesh below it.

Figures 5.44 through 5.51 show the influence of the densified zone properties, width of the treated area (expressed as treatment width/depth ratio), seismic coefficient, and excess pore water pressures in the zone on the predicted stability safety factor and deformations of the pier footing. The following trends in the predicted stability safety factor and maximum displacements are observed:

- Strength and Stiffness (Figures 5.44 and 5.45) – As the strength and stiffness of the densified zone increases, the stability safety factor increases and displacements decrease;
- Width of Treatment (Figures 5.46 and 5.47) – As the width of the treated zone increases (represented by an increasing width to depth ratio where the width is measured outward from the edge of the footing and the depth, which was held

constant at the full-treatment depth of 10 meters, is measured downward from the footing base), the stability safety factor increases and the predicted displacements decrease;

- Seismic Coefficient (Figures 5.48 and 5.49) – As the seismic coefficient (equal to the ratio of the assumed horizontal acceleration induced by the earthquake in the soil mass divided by the downward gravitational acceleration) increases, the stability safety factor decreases and the footing displacements increase.
- Excess Pore Pressure Ratio, r_u (Figures 5.50 and 5.51) – As the excess pore pressure ratio assumed to develop in the densified zone during shaking increases, the stability safety factor decreases and the maximum footing displacements increase.

The trends in both the predicted stability safety factor and maximum horizontal and vertical displacements of the pier footing with changes in the densified zone parameters appears reasonable. As conditions are changed resulting in less system stability, the stability safety factor decreases and the displacements increase. The plots in Figures 5.44 to 5.51 indicate that when the predicted stability safety factor was greater than one the predicted maximum horizontal and vertical footing displacements were less than 5 cm and 2 cm, respectively. These displacements would generally be acceptable for a bridge, as seen from the displacement performance criteria discussed in Chapter 4, Section 4.2.1, and given in Table 4.1.

Despite the logical trend in the stability safety factor and displacements obtained from the pseudostatic analyses, there are several difficulties with the approach and the results obtained. One problem is the method does not account for the progressive accumulation of displacements that occur during shaking. This shortcoming could potentially be corrected by factoring up the predicted displacements by the number of significant cycles of shaking in the design ground motion. Another related problem is difficulty in selecting an appropriate modulus number to use in the hyperbolic model for the analysis. Including a modulus number for virgin loading behavior, as done in the analyses for this study, may produce excessive deformations if the pseudostatic deformations are factored up by the number of significant loading cycles because most of the soil stress-strain behavior under the cyclic earthquake loading is likely unloading and reloading. However, only inputting unloading-reloading modulus numbers could result in

deformations that are too low if the actual loading goes beyond the previous limits and onto the virgin portion of the stress-strain curve.

The pseudostatic approach is also difficult to use due to its inability to model the periodic failure that occurs during shaking and results in accumulated permanent deformations, but not gross failure of the system. As observed in Figures 5.44 to 5.51, as the stability factor of safety decreases below 1.0 the predicted displacements increase at a progressively higher rate. For the cases in Figures 5.47 and 5.49, this ultimately resulted in non-convergence of the deformation analysis when the factor of safety became sufficiently low. In general, conditions producing a pseudostatic stability safety factor less than one should result in a non-convergent pseudostatic deformation analysis because force equilibrium can no longer be maintained by the peak soil strength. Therefore, a pseudostatic deformation analysis can be non-convergent and predict excessively large deformations, even if the failure condition is actually only a transient one that results in limited deformation. For instance, the non-convergence predicted for the width to depth treatment ratio of 0.75 in Figure 5.47 does not result in predicted failure and excessive deformation when analyzed using a coupled, dynamic effective stress analysis of the pier and improved soil system for similar conditions, as described later in Chapter 7.

A pseudostatic deformation analysis can not inherently incorporate the effect of earthquake frequency on the predicted deformation of an improved ground and supported structure system. As discussed in Chapter 3, Riemer et al. (1996) found that the predicted deformation of a highway embankment located over liquefiable soils with ground improvement was less for an earthquake record having a predominant frequency of 10 Hertz (from the 1987 Saguenay Earthquake) than for one with a predominant frequency of 2 Hertz (from the 1989 Loma Prieta Earthquake), even though both records were scaled to the same peak acceleration and soil conditions were identical. Adjusting pseudostatic deformation results to incorporate such a frequency effect would be difficult. Development of such an adjustment would likely require extensive parametric studies to be performed and extensive testing of the method to verify its accuracy.

Finally, selection of a seismic coefficient to use in pseudostatic stability and deformation analyses that is representative of a non-uniform earthquake motion is difficult. The predictions from those analyses are directly dependent on the coefficient selected, making the value used critical.

5.4.5 Assessment of Pseudostatic Approach

As seen from the results discussed above, pseudostatic stability and deformation analyses can provide the engineer with a relative assessment of the performance obtained using different ground improvement schemes for support of a structure in liquefiable soil deposits. However, the pseudostatic approach does not adequately model some of the fundamental mechanisms controlling permanent movements of an improved ground and supported structure system. Therefore, the stability safety factors and deformations predicted by pseudostatic methods, particularly those investigated as part of this research, can not be used to quantitatively assess performance. Quantitative assessments of performance can probably be more effectively performed using coupled, dynamic analyses that more correctly incorporate many of the factors and phenomena influencing the behavior of an improved ground and supported structure system within a liquefiable deposit.

5.5 Implications for Prediction of Performance

The various methods investigated for predicting improved ground performance using an uncoupled analytical approach have provided useful insights regarding the feasibility of such an approach, as well as the behavior of treated ground systems in general. The results of the analyses performed indicate:

- Significant ground accelerations, pore pressure increments, and deformation increments in an improved zone may occur at a time, prior to complete liquefaction of surrounding untreated soils, when the treated-untreated soil system softens to the point of having a first natural period close to the predominant period of the input motion;
- Pore pressures that develop in a densified zone during and after shaking are highly dependent on the duration of the earthquake, relative hydraulic conductivities and compressibilities of the treated and untreated soil, the drainage boundary conditions, and the presence of 3-D versus 2-D conditions; and
- Pseudostatic stability and deformation analyses can provide a qualitative assessment of the relative performance of improved ground schemes in some cases, but can not

be used to quantitatively predict performance based on the computed stability safety factors and movements.

The results from the simplified analyses performed indicate the complex nature of the behavior of an improved ground zone and supported structure located within liquefiable soil, and the potential interdependence of the phenomena influencing that behavior. Correctly evaluating the performance of an improved ground and supported structure system using a series of uncoupled analyses does not appear feasible. A coupled analytical method incorporating the important factors controlling the system behavior is likely the preferred approach for predicting performance. Such an approach was investigated, verified, and adopted for conducting parametric studies of the effectiveness of ground improvement for liquefaction mitigation at existing highway bridges, as discussed in the next chapter.

TABLE 5.1: Properties Used for Loose and Dense Sands in QUAD4M Analyses

Property	Loose Sand (D_r = 40%)	Dense Sand (D_r = 90%)
Total Unit Weight [1] (kN/m^3)	19.4, 19.9	20.4, 20.9
Poisson's Ratio	0.35, 0.45 [2]	0.35
Shear Modulus Number, K_{2max} [3]	35, 41 [4]	70
Reduced Shear Modulus [5] (kPa)	20, 65, 150, 352, 1000	-
Damping Ratio for Sand in Non-liquefied State	Per Idriss (1990)	Per Idriss (1990)
Damping Ratio for Sand in Liquefied State [6] (%)	10, 25, 40	-

Notes:

1. First and second unit weights are saturated unit weights with water and glycerin-water, respectively.
2. Poisson's ratio of 0.45 only used for cases where loose sand treated as liquefied and assigned a constant, reduced shear modulus.
3. Shear modulus number used to compute maximum shear modulus, G_{max}, using formula proposed by Seed and Idriss (1970) where $G_{max} = 1000\ K_{2max}\ (\sigma_m')^{0.5}$ and σ_m' is mean effective confining stress, with both G_{max} and σ_m' having units of pounds per square foot (psf). G_{max} then used with modulus degradation values proposed by Idriss (1990).
4. Loose sand K_{2max} of 41 used for all analyses where loose zone not considered to be liquefied, with exception of case of glycerin-water pore fluid where two separate analyses performed using K_{2max} of 41 and 35. In figures 5.5 to 5.28 loose zone shear modulus of 20,000 and 17,000 kPa were approximate average shear moduli in loose zone during analyses performed using K_{2max} values of 41 and 35, respectively, for loose sand along with modulus degradation curves.
5. Reduced shear moduli used for analyses where loose sand considered to be completely liquefied throughout shaking. The reduced modulus was assumed to be constant (no modulus degradation curves used).
6. Constant damping ratio assumed for loose sand considered to be completely liquefied throughout shaking.

TABLE 5.2: Shear Modulus Reduction Factor, G/G_{max}, and Damping Ratio for Sand at Different Strain Levels from Idriss (1990)

Shear Strain (%)	G/G_{max}	Damping Ratio (%)
0.0001	1.0	0.24
0.0003	1.0	0.42
0.001	0.99	0.8
0.003	0.96	1.4
0.01	0.85	2.8
0.03	0.64	5.1
0.1	0.37	9.8
0.3	0.18	15.5
1.0	0.08	21

TABLE 5.3: Soil Properties Reported by Iai et al. (1988) for Model Study

Soil Property	Loose Sand	Dense Sand
Permeability, k (cm/sec)	1.06×10^{-2}	5.54×10^{-3}
Volume Compressibility, m_v (cm^2/kg-force)	0.1	0.02

TABLE 5.4: Soil Properties Used for Modeling Study (after Schaeffer, 1998)

Soil Property	Loose Sand	Dense Sand
Saturated Unit Weight, γ_{sat} (kN/m^3)	19.0	20.3
Hydraulic Conductivity, k (m/sec)	6.0×10^{-5}	3.0×10^{-5}
Specific Storage, S_s (m^{-1})	1.0×10^{-4}	3.0×10^{-5}

TABLE 5.5: Forces and Moments Acting at Bottom of Pier Column Based on AASHTO Group I Service Loads

Load Component at Bottom of Column	Load Components by Direction [1,2]	
	Longitudinal	Transverse
Vertical Force (kN) [3]	1496	-
Horizontal Force (kN)	104	53
Moment (kN-m)	27	123

Notes: 1. Longitudinal refers to loading in direction of longitudinal axis of bridge and transverse refers to loading in direction at right angle to longitudinal axis.
2. Longitudinal and transverse components act simultaneously.
3. Vertical load consists of 978 kN of dead load and 518 kN of live load.

TABLE 5.6: Forces and Moments Acting on Stub Abutment Based on AASHTO Group I Service Loads

Load Component on Stub Abutment	Load Components by Direction [1]	
	Longitudinal	Transverse
Vertical Force (kN) [2]	1294	-
Horizontal Force (kN) [3]	0	0
Moment (kN-m) [3]	0	0

Notes: 1. Longitudinal refers to loading in direction of longitudinal axis of bridge and transverse refers to loading in direction at right angle to longitudinal axis.
2. Vertical load consists of 776 kN of dead load and 518 kN of live load.
3. Roller bearings assumed to support beams at stub abutment. Longitudinal and transverse horizontal forces and moments assumed to be small.

TABLE 5.7: Forces and Moments Acting at Bottom of Pier Column Based on AASHTO Group VII Service Loads for Primary Loading in Longitudinal Direction

Load Component at Bottom of Column	Load Components by Direction [1,2,3]	
	100% Longitudinal	30% Transverse
Vertical Force (kN)	978	-
Horizontal Force (kN)	269	115
Moment (kN-m)	654	206

Notes:
1. Longitudinal refers to direction of longitudinal axis of bridge and transverse refers to direction at right angle to longitudinal axis.
2. For earthquake loading evaluation AASHTO (1996) Standard Specification for Highway Bridges, Division I-A (Seismic Design), Section 3.9 specifies following two cases to be evaluated: (a) 100% of load from design earthquake acting in longitudinal direction and 30 % of load from design earthquake acting in transverse direction, (b) 100% of load from earthquake acting in transverse direction and 30% of load from earthquake acting in longitudinal direction. Only case (a) evaluated in these analyses. In both cases longitudinal and transverse loading components are assumed to act simultaneously.
3. Loads shown correspond to seismic coefficient of approximately 0.15 to 0.2.

TABLE 5.8: Equivalent Forces or Stresses at Bottom of Footing for Use in Two-Dimensional Pseudostatic Analyses of Pier Subjected to Longitudinal Seismic Loading

Type of Replacement	Magnitude[1]
Applied force with Eccentricity:	
Vertical force [2]	266 kN/m
Horizontal force [2]	80 kN/m
Eccentricity [3]	0.95 m
Applied Stress over Limited Width:	
Normal stress [4]	127 kPa/m
Shear stress [4]	38 kPa/m
Width of application [5]	2.1 m

Notes: 1. Units of kN/m or kPa/m indicate that force or stress is applied per meter length of footing.
2. Forces shown do not include weight of footing.
3. Eccentricity is relative to the centroid of the footing, which is located at 2 meters from either edge of the 4-meter-wide footing. Eccentricity shown does not account for impact of footing weight on resultant forces.
4. Stresses shown do not include those induced by footing weight.
5. Normal and shear stresses are applied over a width extending from the footing edge to a distance 2.1 meters inward from the edge.

TABLE 5.9: Cases Evaluated and Parameter Values Used in Pseudostatic Stability Analyses

Case No.	Parameter Varied	Densified Zone Properties [1]	Width/Depth Ratio of Zone [2], W/D	Seismic Coefficient, S [3]	Excess Pore Pressure Ratio [4], r_u	Figure Presenting Results
1	Densified zone properties	ϕ' = 32, 35, 38, 40 degrees γ = 19, 19.5, 20, 20.5 kN/m^3	1.0	0.2	0.2	5.44
2	Width/depth ratio of zone	ϕ' = 38 degrees γ = 20 kN/m^3	0.75, 1.0, 1.5	0.2	0.2	5.46
3	Seismic Coefficient, S	ϕ' = 38 degrees γ = 20 kN/m^3	1.0	0.1, 0.2, 0.25, 0.3, 0.35, 0.4	0.2	5.48
4	Excess pore pressure ratio, r_u	ϕ' = 38 degrees γ = 20 kN/m^3	1.0	0.2	0.0, 0.2, 0.4	5.50

Notes:

1. For Case 1 the values for ϕ' and γ are paired together in the order which they appear in their respective lists (i.e. – ϕ' of 32^o is paired with γ of 19 kN/m^3, ϕ' of 35^o is paired with γ of 19.5 kN/m^3)
2. Width is defined as distance of densified zone extending beyond edge of footing and depth is distance of treatment beneath bottom of footing. In all cases, full 10-meter depth of liquefied soil beneath footing was treated and only real variable was width.
3. Seismic coefficient is equal to ratio of assumed horizontal acceleration induced by earthquake in soil mass divided by gravitational acceleration.
4. Excess pore pressure ratio is assumed to be uniform throughout densified zone.

TABLE 5.10: Cases Evaluated and Parameter Values Used in Pseudostatic Deformation Analyses

Case No.	Parameter Varied	Densified Zone Properties [1, 2]	Width/Depth Ratio of Zone [3], W/D	Seismic Coefficient [4], S	Excess Pore Pressure Ratio [5], r_u	Figure Presenting Results
1	Densified zone properties	K = 350, 450, 625, 800 K_{ur} = 608, 765, 1062,1360 K_b = 146, 167, 217, 267 ϕ' = 32, 35, 38, 40 degrees γ' = 9.4, 9.9, 10.5, 11.4 kN/m^3 Constant values: n = 0.45, m = 0.45, R_f = 0.7	1.0	0.2	0.2	5.45
2	Width/depth ratio of zone	K = 450, K_{ur} = 1062, K_b = 217, R_f = 0.7, n = 0.45, m = 0.45, ϕ' = 38, γ' = 10.5 kN/m^3	0.75, 1.0, 1.5	0.2	0.2	5.47
3	Seismic Coefficient, S	K = 450, K_{ur} = 1062, K_b = 217, R_f = 0.7, n = 0.45, m = 0.45, ϕ' = 38, γ' = 10.5 kN/m^3	1.0	0.1, 0.2, 0.25, 0.3, 0.35, 0.4	0.2	5.49
4	Excess pore pressure ratio, r_u	K = 450, K_{ur} = 1062, K_b = 217, R_f = 0.7, n = 0.45, m = 0.45, ϕ' = 38, γ' = 10.5 kN/m^3	1.0	0.2	0.0, 0.2, 0.4	5.51

Notes:

1. Densified soil properties include hyperbolic model parameters (K, K_{ur}, K_b, R_f, n, and m), strength parameters (ϕ'), and buoyant unit weight (γ'). K is Young's modulus coefficient, K_{ur} is Young's modulus coefficient for unloading and reloading, K_b is bulk modulus coefficient, R_f is failure ratio, n is Young's modulus exponent, and m is bulk modulus exponent. ϕ' is effective friction angle. γ' given is for r_u = 0; for higher r_u, γ' was appropriately reduced.
2. For Case 1 the values for K, K_{ur}, K_B, ϕ', and γ' are grouped together in the order which they appear in their respective lists (i.e. – K = 625, K_{ur} = 1062, K_b = 217, ϕ' = 38^o, and γ' = 10.5 kN/m^3 are grouped together). Values of R_f, n, and m are the same in all analyses.
3. Width is defined as distance of densified zone extending beyond edge of footing and depth is distance of treatment beneath bottom of footing. In all cases, full 10-meter depth of liquefied soil beneath footing was treated and only real variable was width.
4. Seismic coefficient given is for use with total unit weight of soil. S in analysis was factored up to account for use of buoyant unit weight.
5. Excess pore water pressure ratio is assumed to be uniform throughout densified zone.

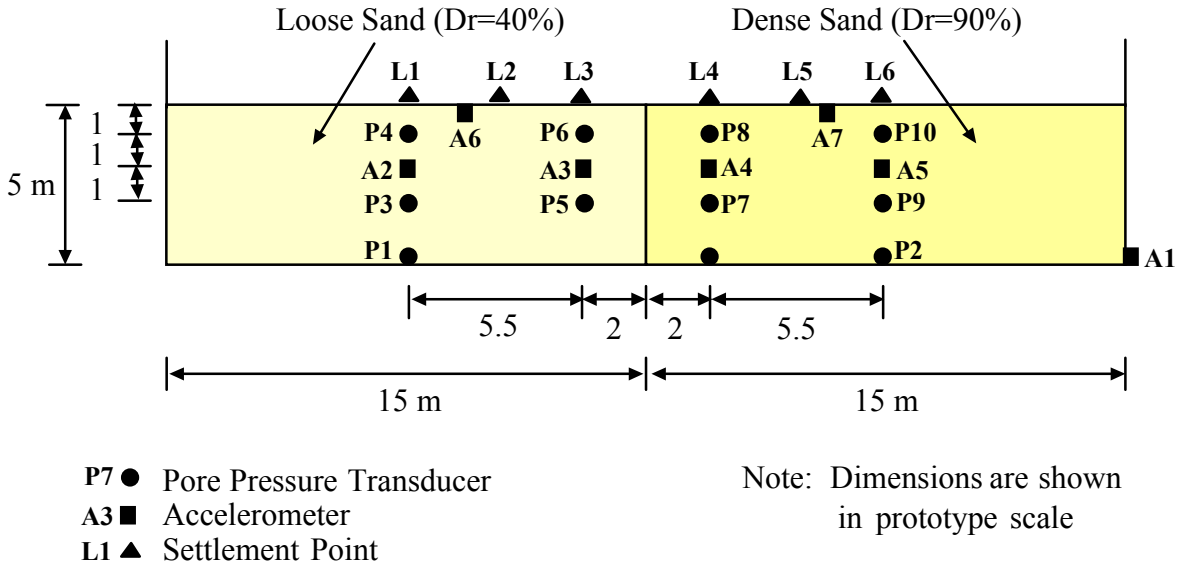

FIGURE 5.1: Adjacent Loose/Dense Sand Zones in Centrifuge Test by Adalier (after Adalier, 1996)

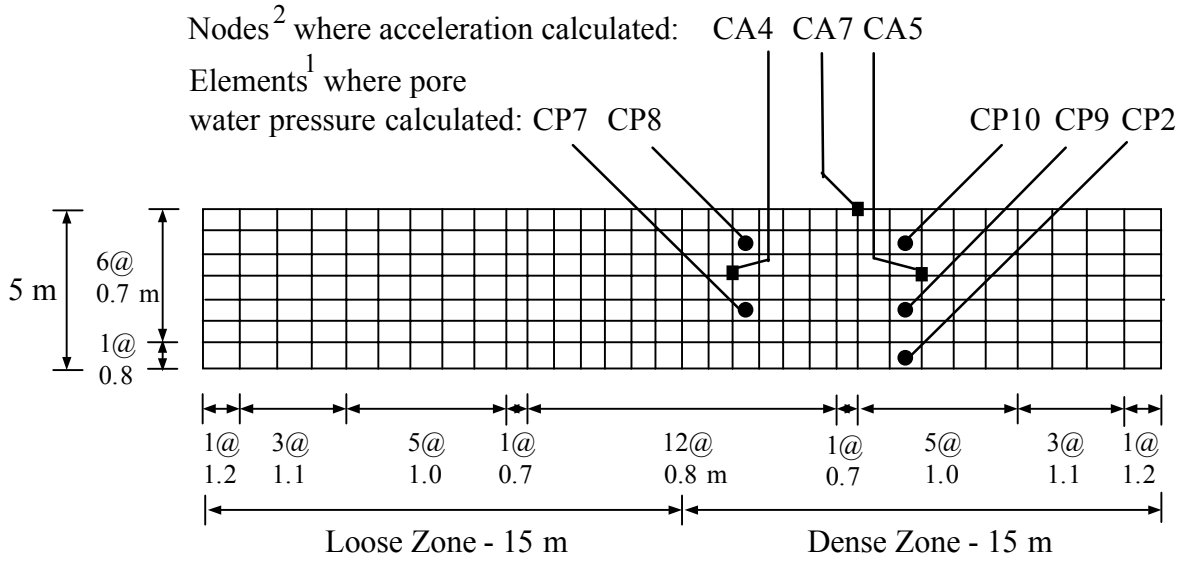

Note: 1. Element designation is same as pore pressure transducer designation shown in Figure 5.1 with prefix C added.
2. Node designation is same as accelerometer designation shown in Figure 5.1 with prefix C added.

FIGURE 5.2: Coarse Mesh Used in QUAD4M Analyses

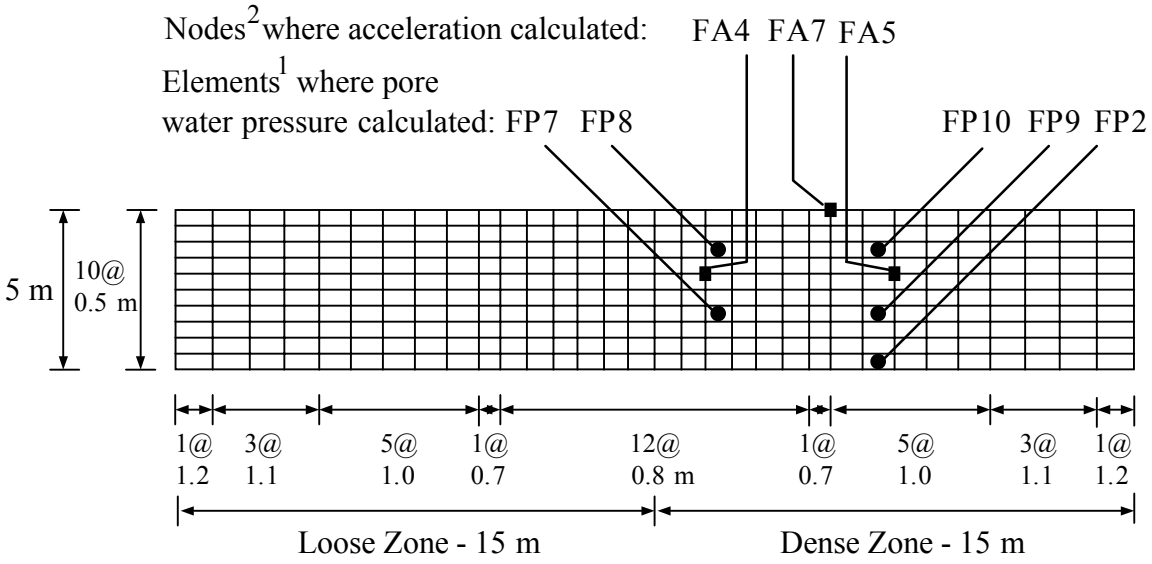

Note: 1. Element designation is same as pore pressure transducer designation shown in Figure 5.1 with prefix F added.
2. Node designation is same as accelerometer designation shown in Figure 5.1 with prefix F added.

FIGURE 5.3: Fine Mesh Used in QUAD4M Analyses

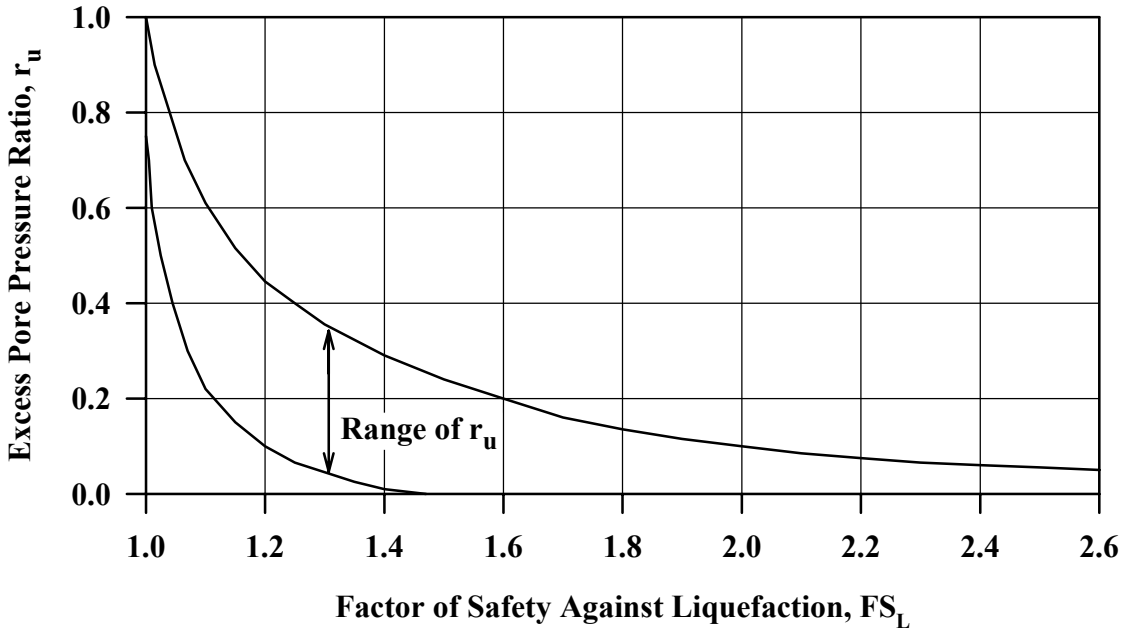

FIGURE 5.4: Typical Relationship Between Residual Excess Pore Pressure Ratio and Factor of Safety Against Liquefaction for Sand (after Marcuson & Hynes, 1987 as presented by Seed & Harder, 1990)

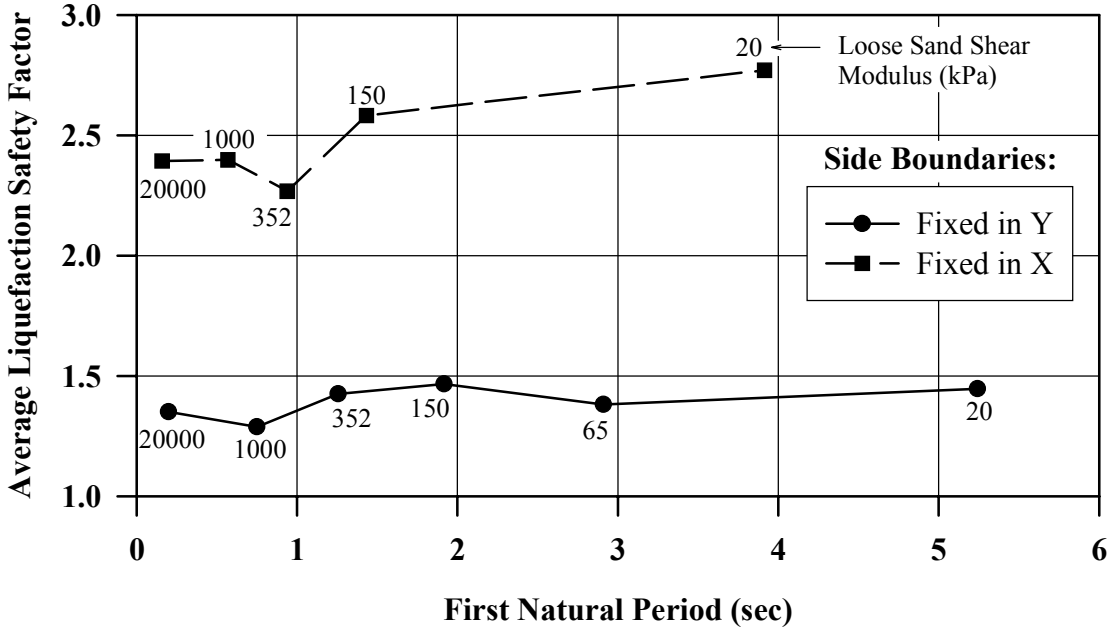

FIGURE 5.5: Variation of Predicted Liquefaction Safety Factor for Dense Zone with System Period for Different Side Boundaries

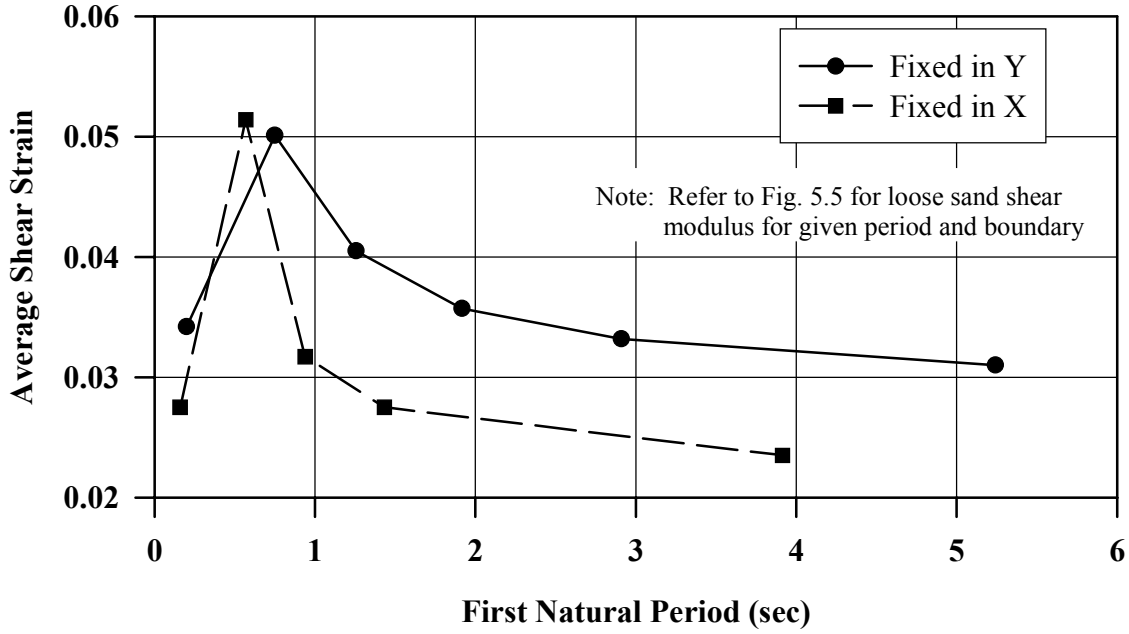

FIGURE 5.6: Variation of Predicted Shear Strain for Dense Zone with System Period for Different Side Boundaries

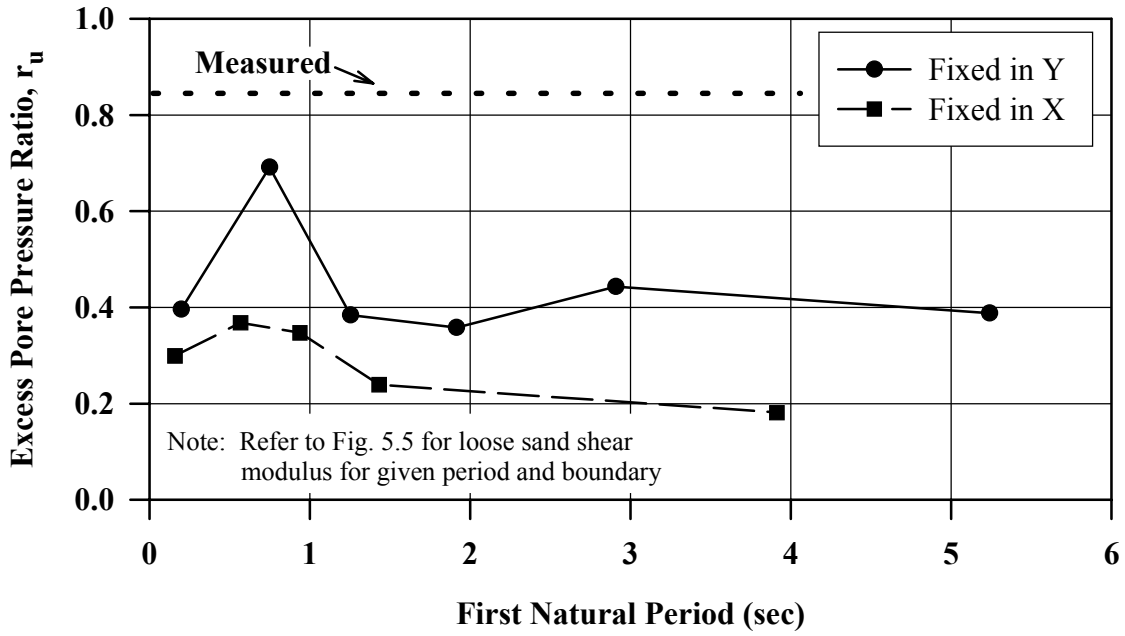

FIGURE 5.7: Variation of Predicted Excess Pore Pressure Ratio at CP7 in Dense Zone with System Period for Different Side Boundaries

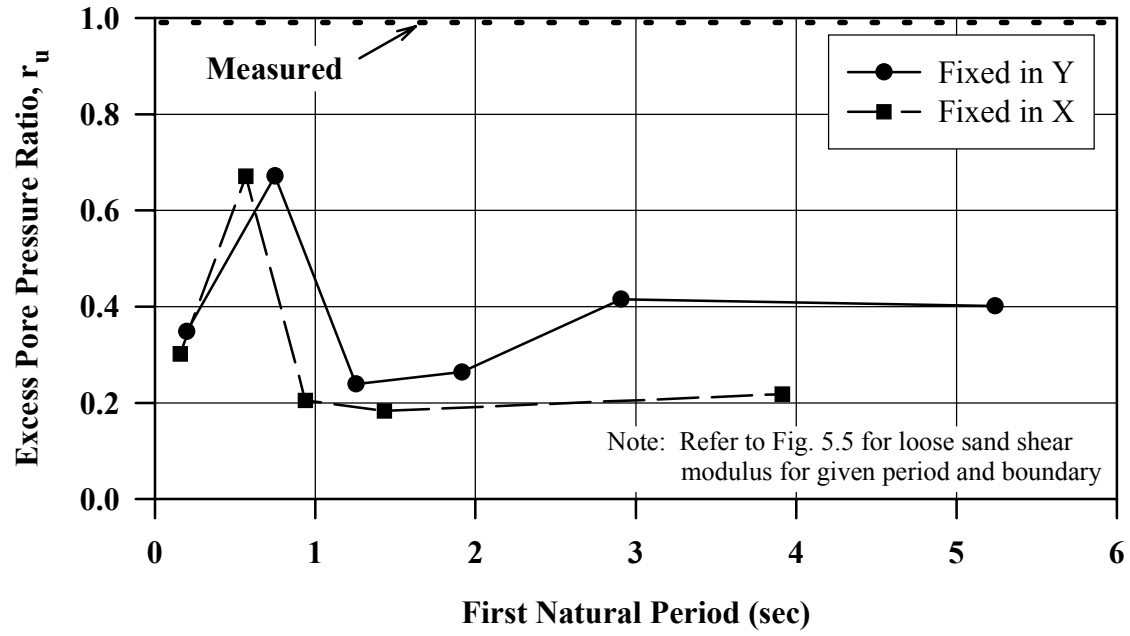

FIGURE 5.8: Variation of Predicted Excess Pore Pressure Ratio at CP8 in Dense Zone with System Period for Different Side Boundaries

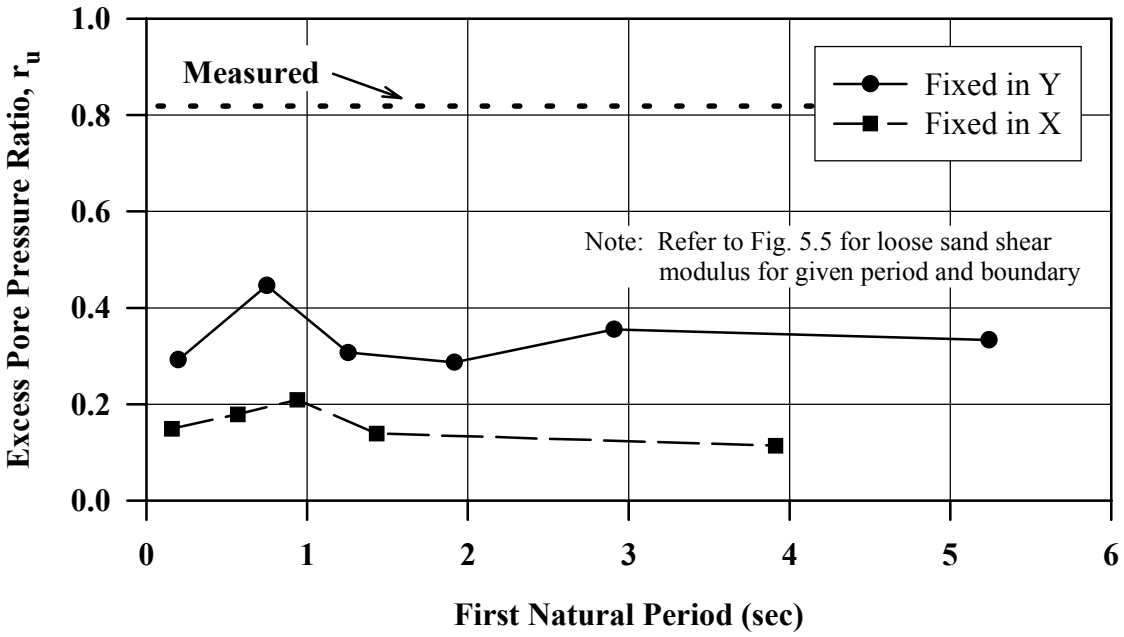

FIGURE 5.9: Variation of Predicted Excess Pore Pressure Ratio at CP2 in Dense Zone with System Period for Different Side Boundaries

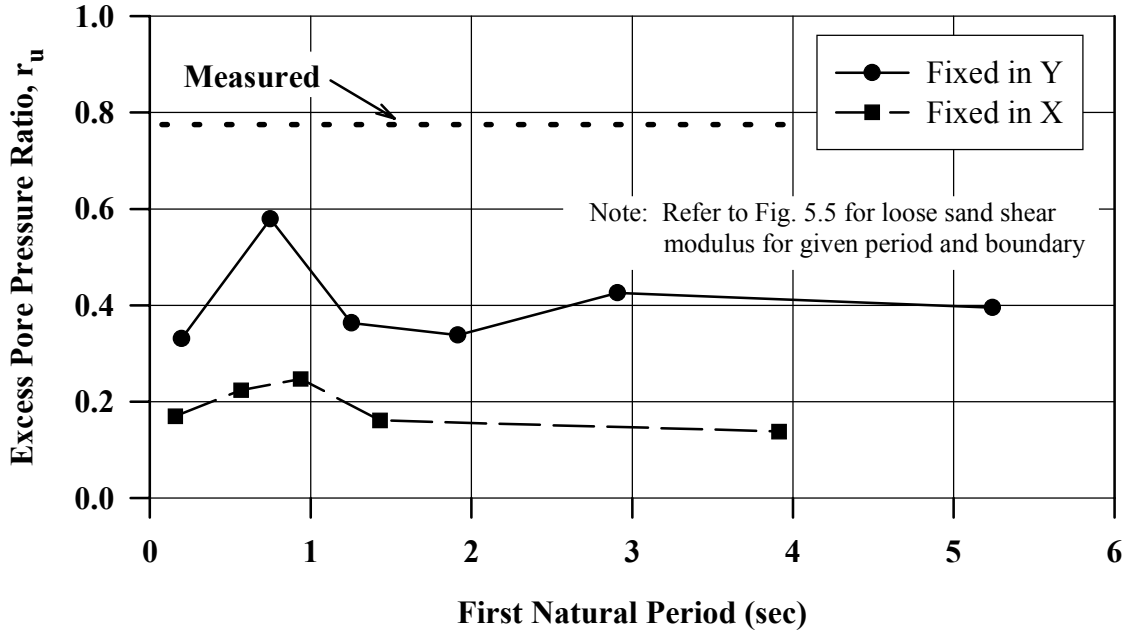

FIGURE 5.10: Variation of Predicted Excess Pore Pressure Ratio at CP9 in Dense Zone with System Period for Different Side Boundaries

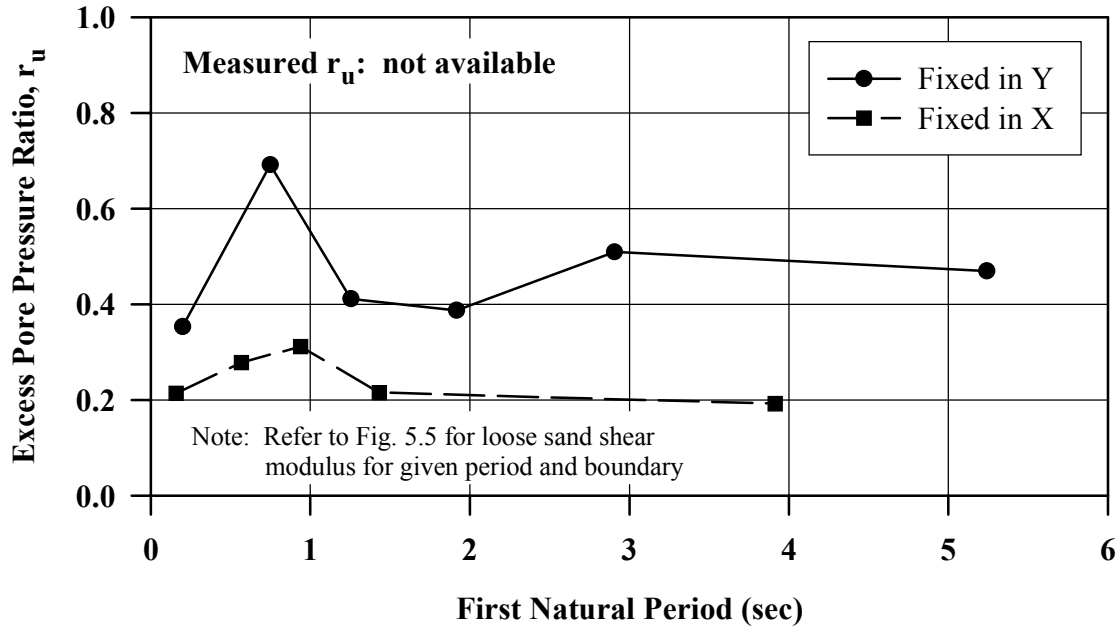

FIGURE 5.11: Variation of Predicted Excess Pore Pressure Ratio at CP10 in Dense Zone with System Period for Different Side Boundaries

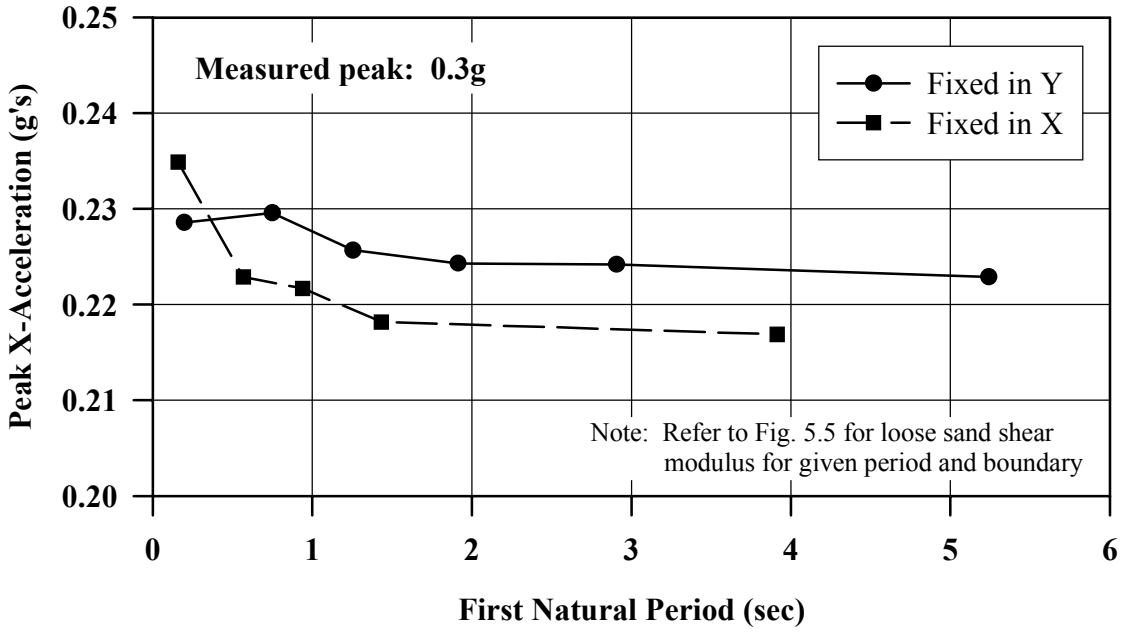

FIGURE 5.12: Variation of Predicted Peak X-Acceleration at CA4 in Dense Zone with System Period for Different Side Boundaries

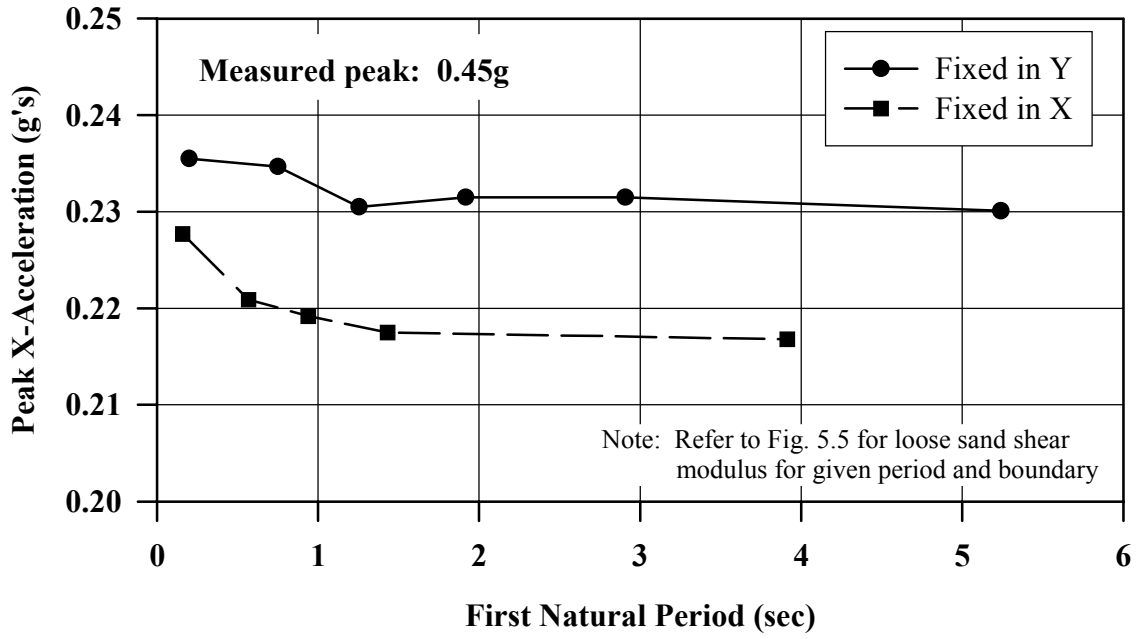

FIGURE 5.13: Variation of Predicted Peak X-Acceleration at CA7 in Dense Zone with System Period for Different Side Boundaries

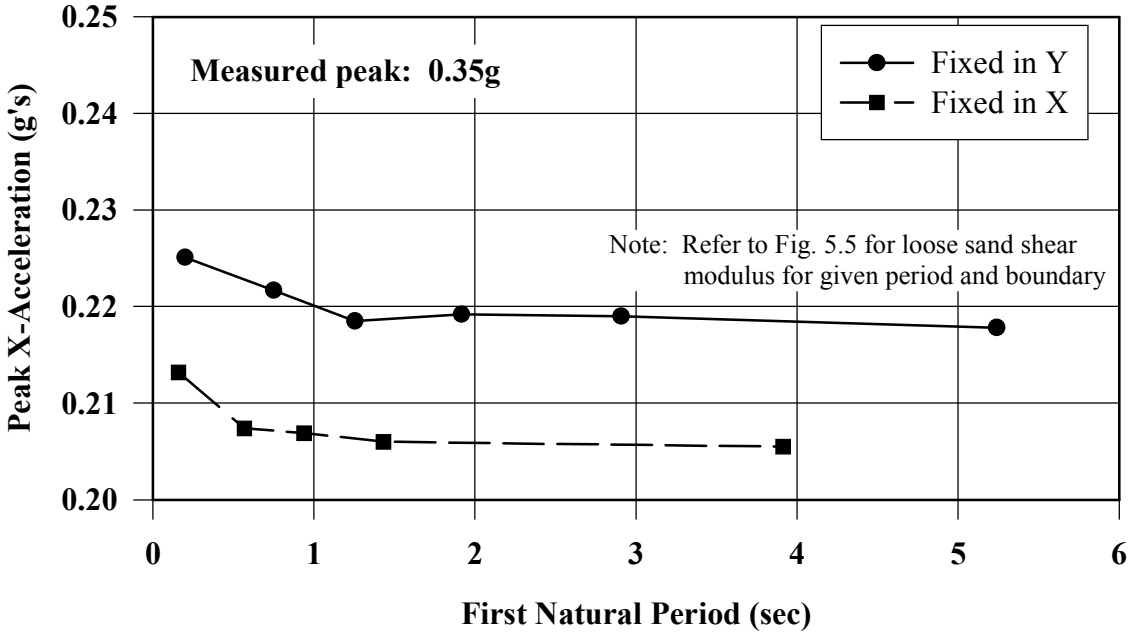

FIGURE 5.14: Variation of Predicted Peak X-Acceleration at CA5 in Dense Zone with System Period for Different Side Boundaries

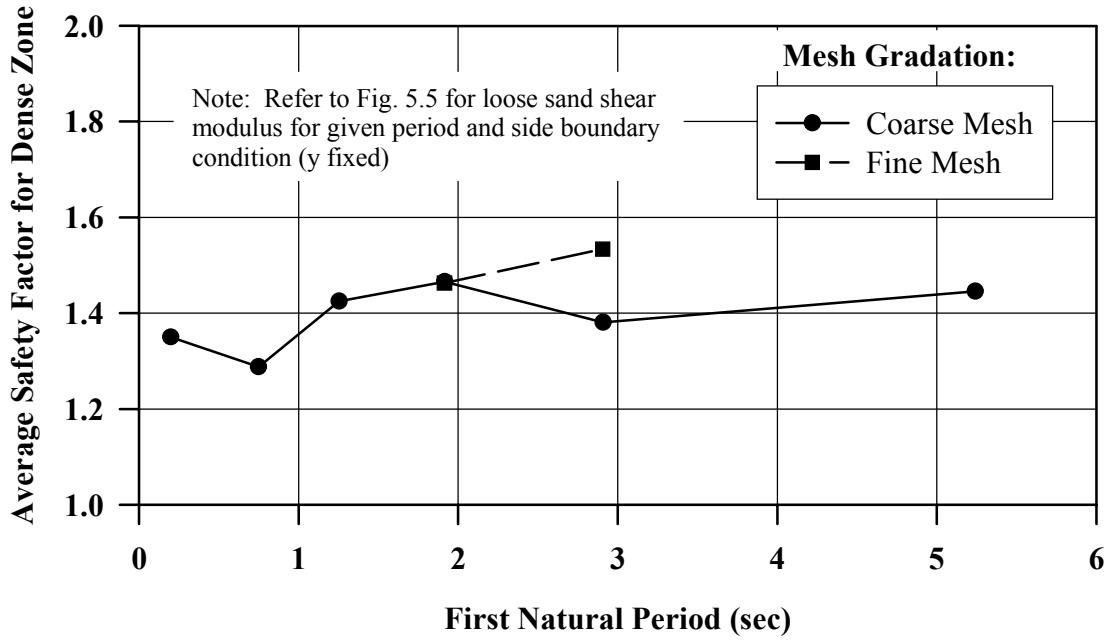

FIGURE 5.15: Effect of Mesh Gradation on Predicted Liquefaction Safety Factor for Dense Zone

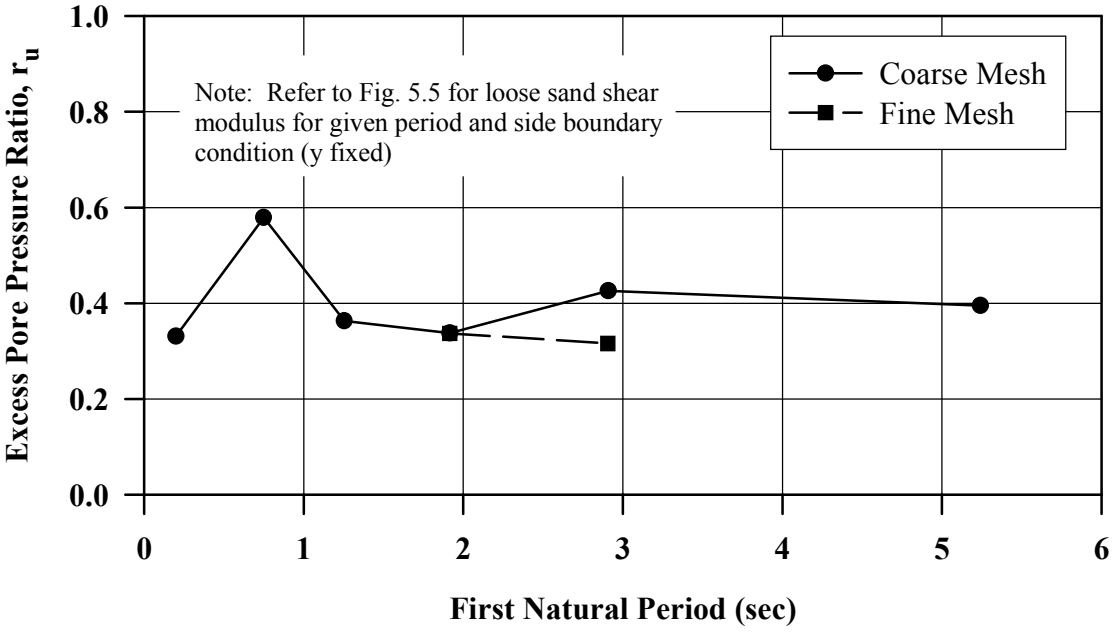

FIGURE 5.16: Effect of Mesh Gradation on Predicted Excess Pore Pressure Ratio at CP9 in Dense Zone

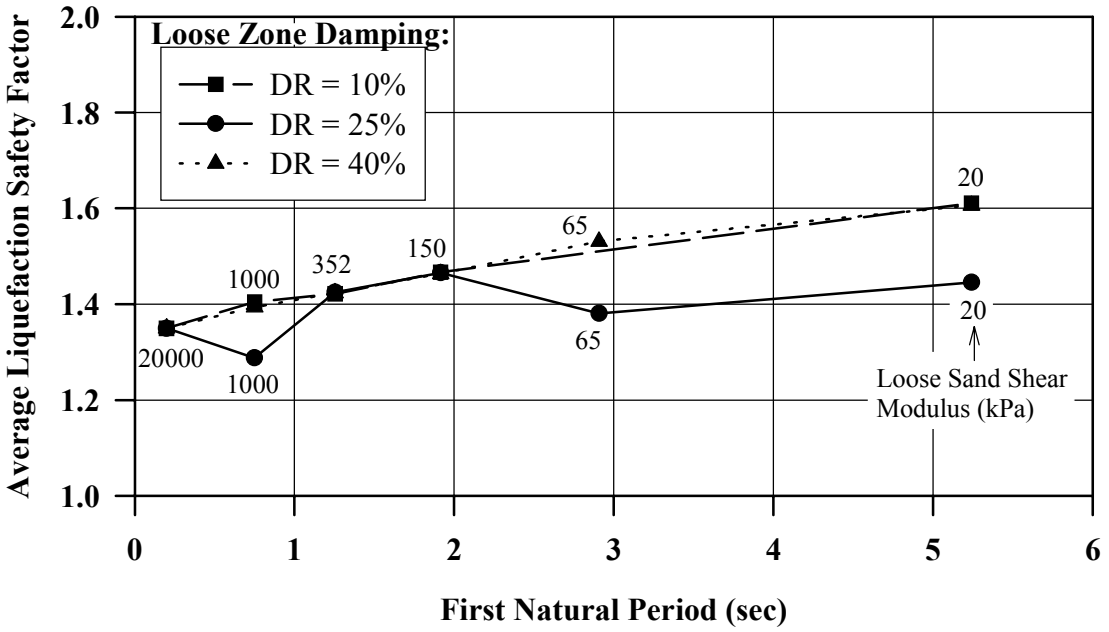

FIGURE 5.17: Variation of Predicted Liquefaction Safety Factor for Dense Zone with System Period for Different Damping Ratios (DR)

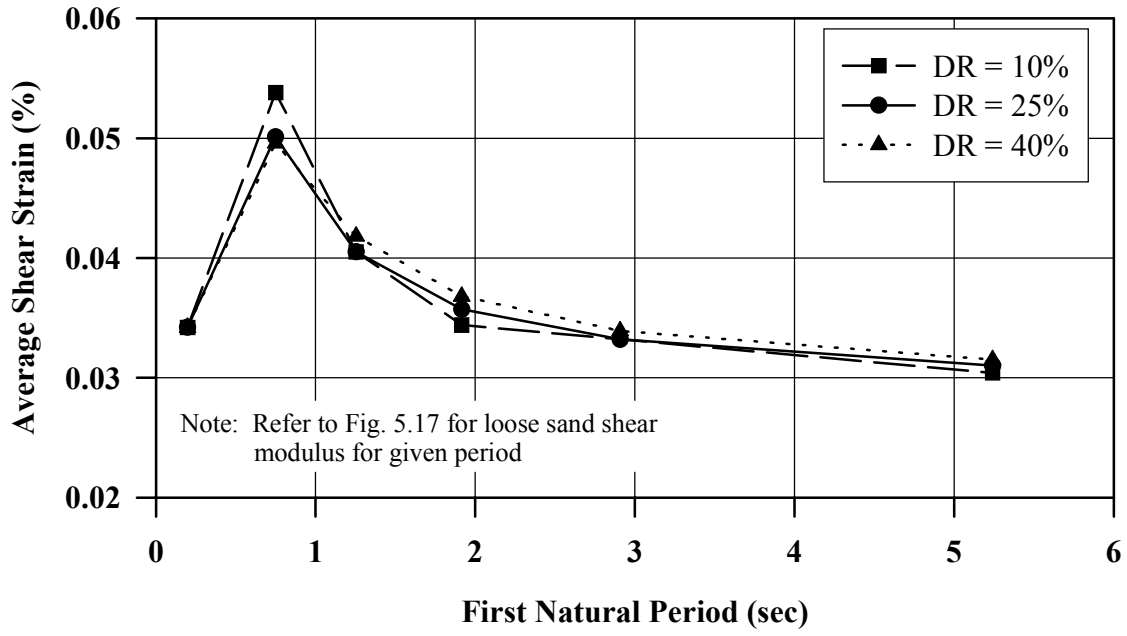

FIGURE 5.18: Variation of Predicted Shear Strain for Dense Zone with System Period for Different Damping Ratios (DR)

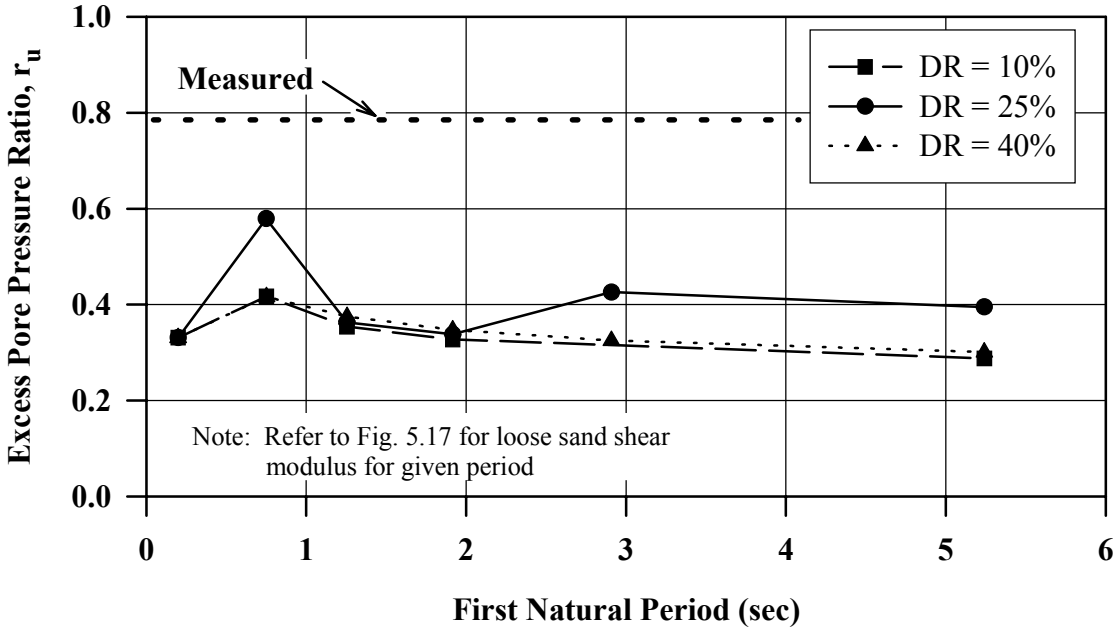

FIGURE 5.19: Variation of Predicted Excess Pore Pressure Ratio at CP9 in Dense Zone with System Period for Different Damping Ratios (DR)

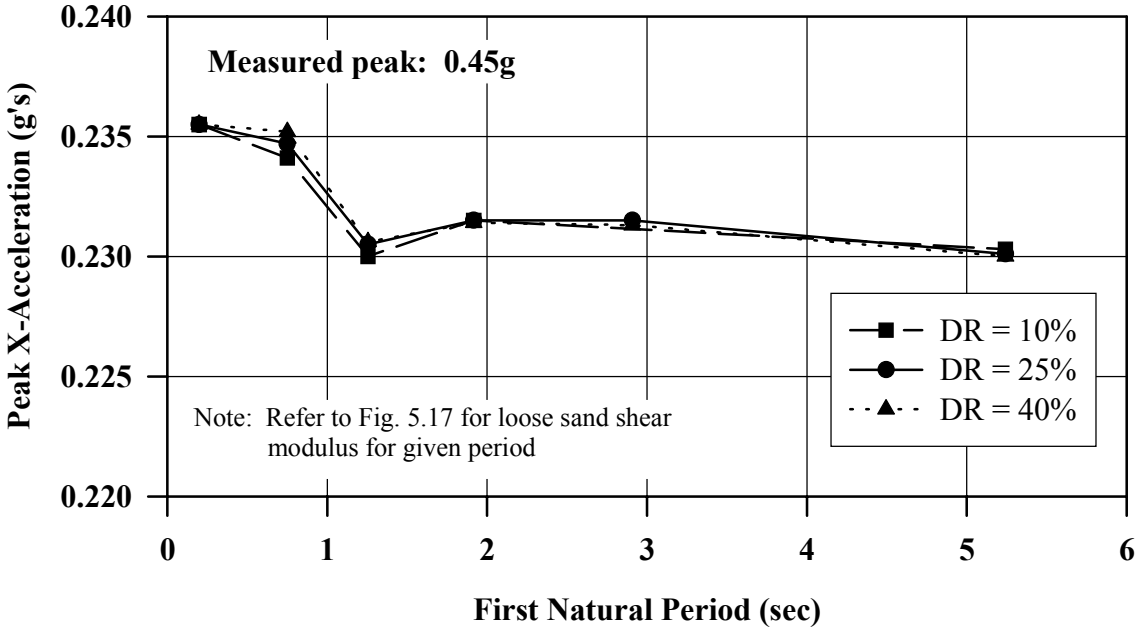

FIGURE 5.20: Variation of Predicted Peak X-Acceleration at CA7 in Dense Zone with System Period for Different Damping Ratios (DR)

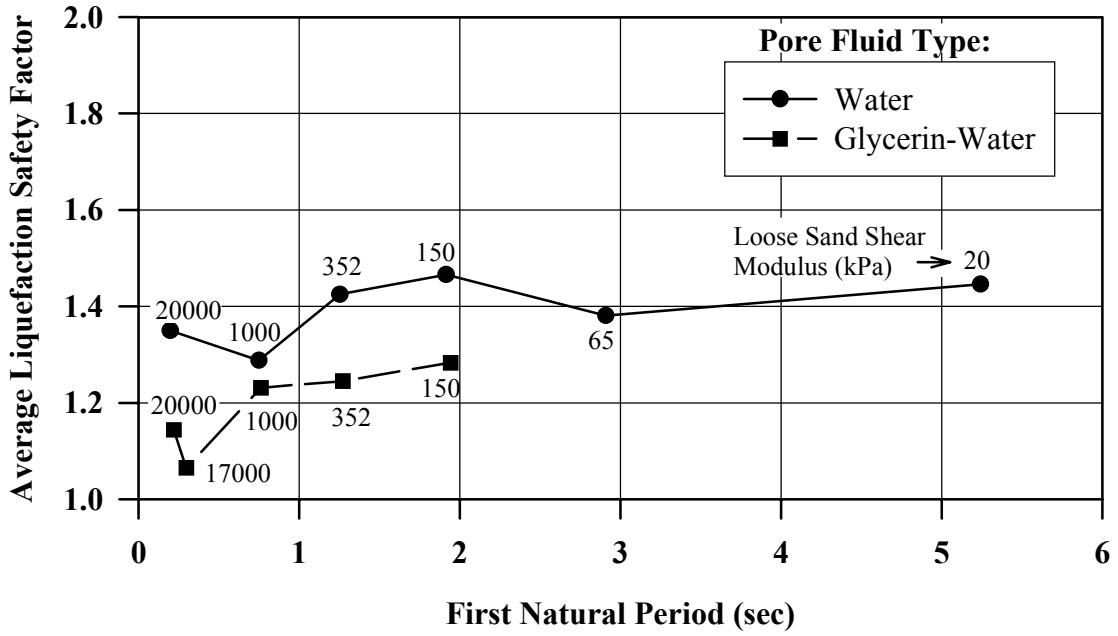

FIGURE 5.21: Variation of Predicted Liquefaction Safety Factor for Dense Zone with System Period for Different Pore Fluids

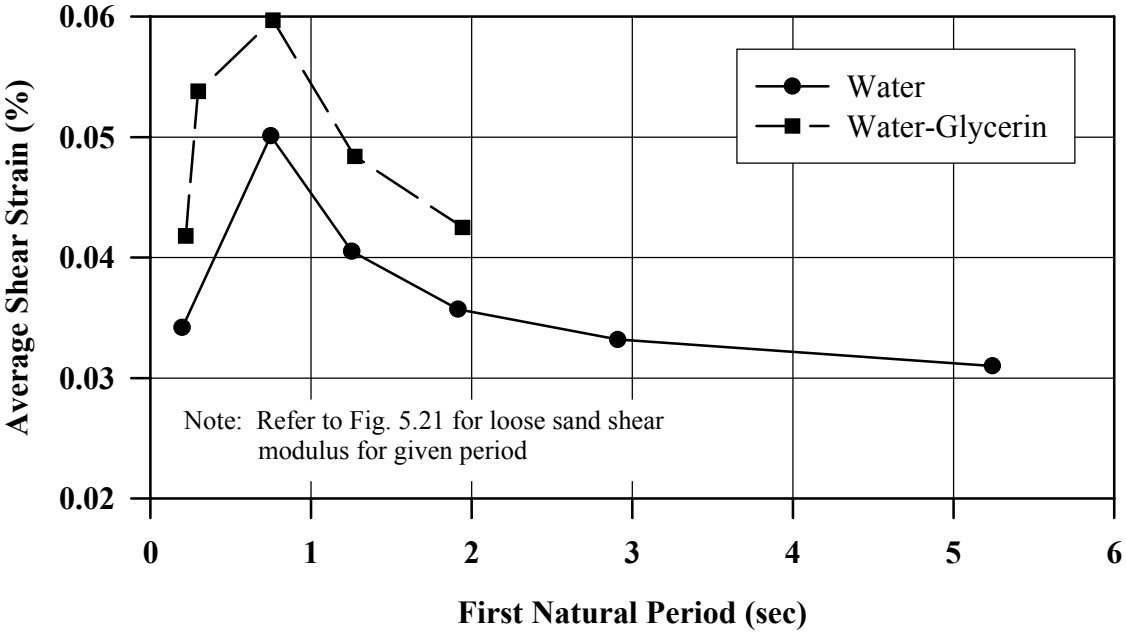

FIGURE 5.22: Variation of Predicted Shear Strain for Dense Zone with System Period for Different Pore Fluids

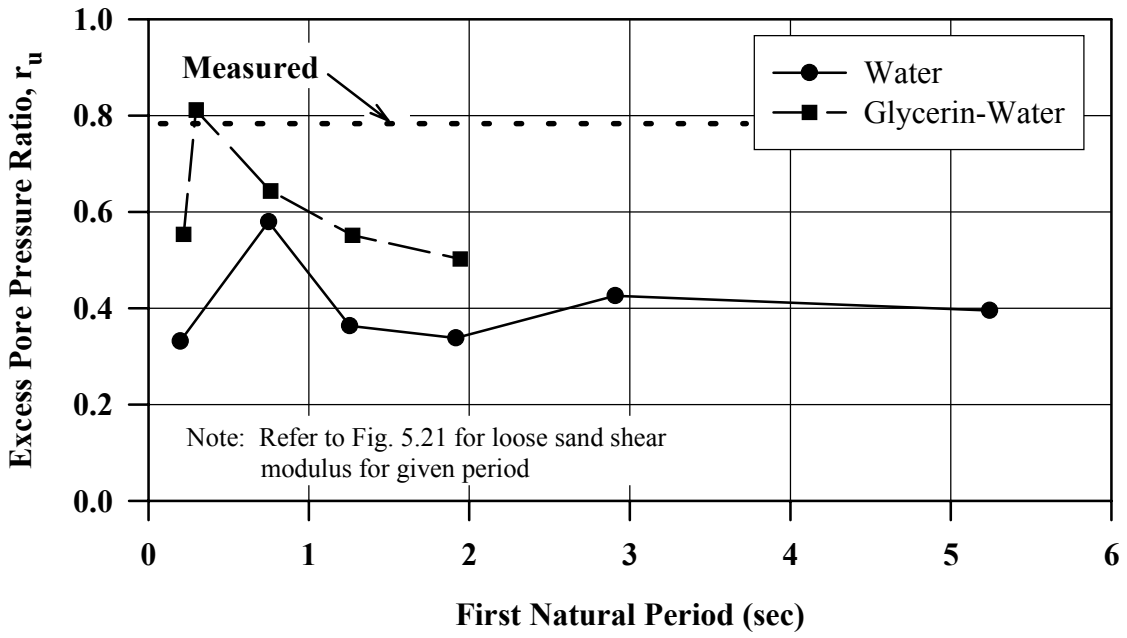

FIGURE 5.23: Variation of Predicted Excess Pore Pressure Ratio at CP9 in Dense Zone with System Period for Different Pore Fluids

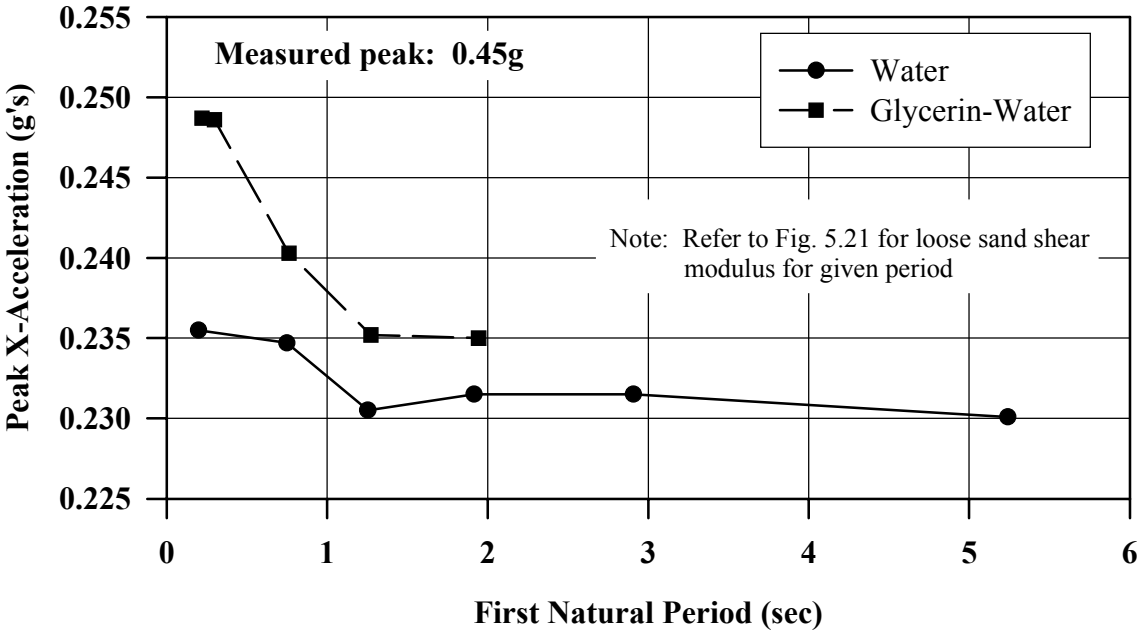

FIGURE 5.24: Variation of Predicted Peak X-Acceleration at CA7 in Dense Zone with System Period for Different Pore Fluids

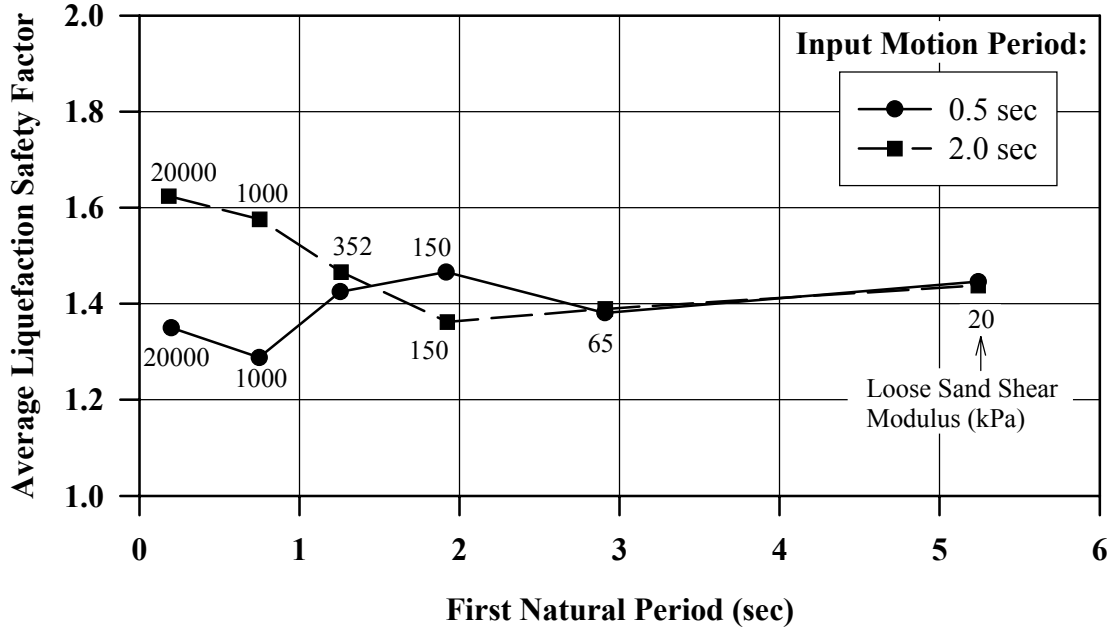

FIGURE 5.25: Variation of Predicted Liquefaction Safety Factor for Dense Zone with System Period for Different Input Motion Periods

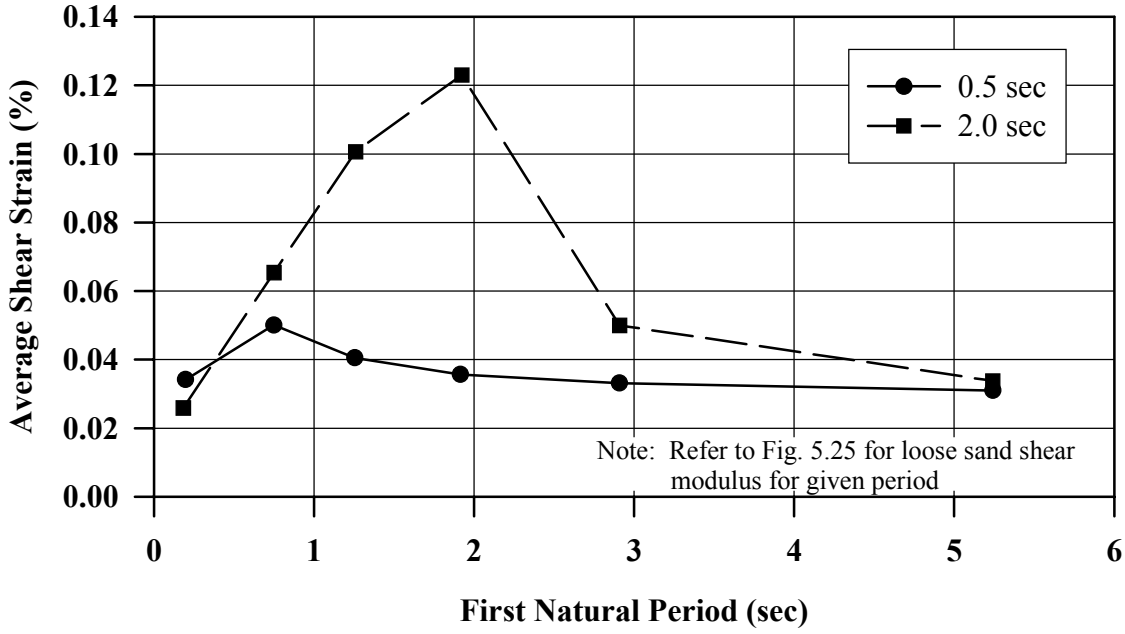

FIGURE 5.26: Variation of Predicted Shear Strain for Dense Zone with System Period for Different Input Motion Periods

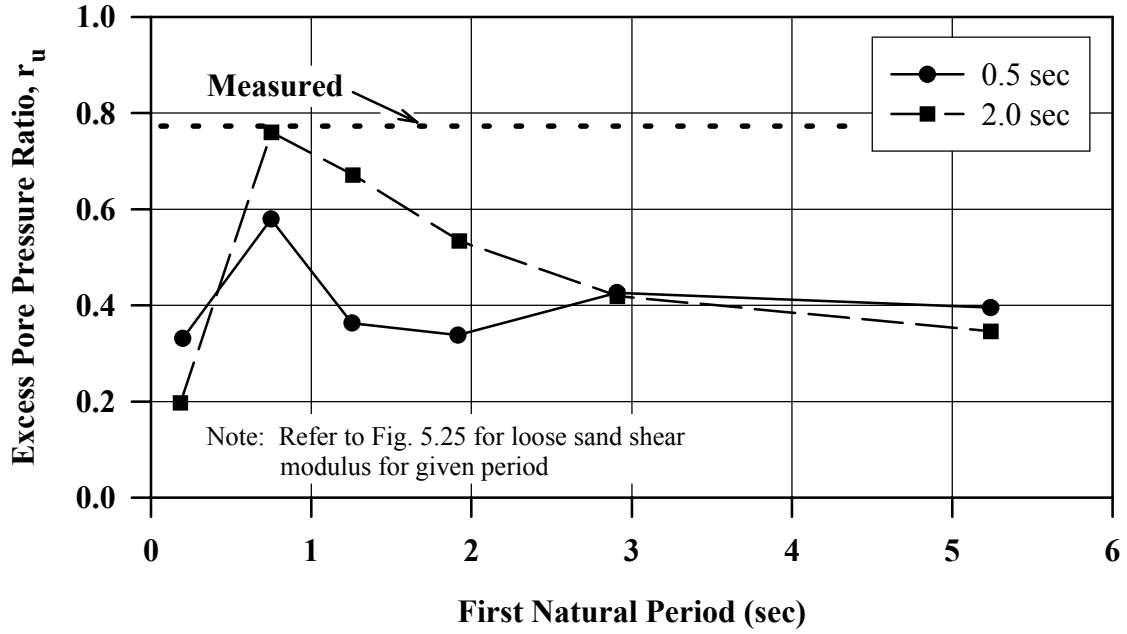

FIGURE 5.27: Variation of Predicted Excess Pore Pressure Ratio at CP9 in Dense Zone with System Period for Different Input Motion Periods

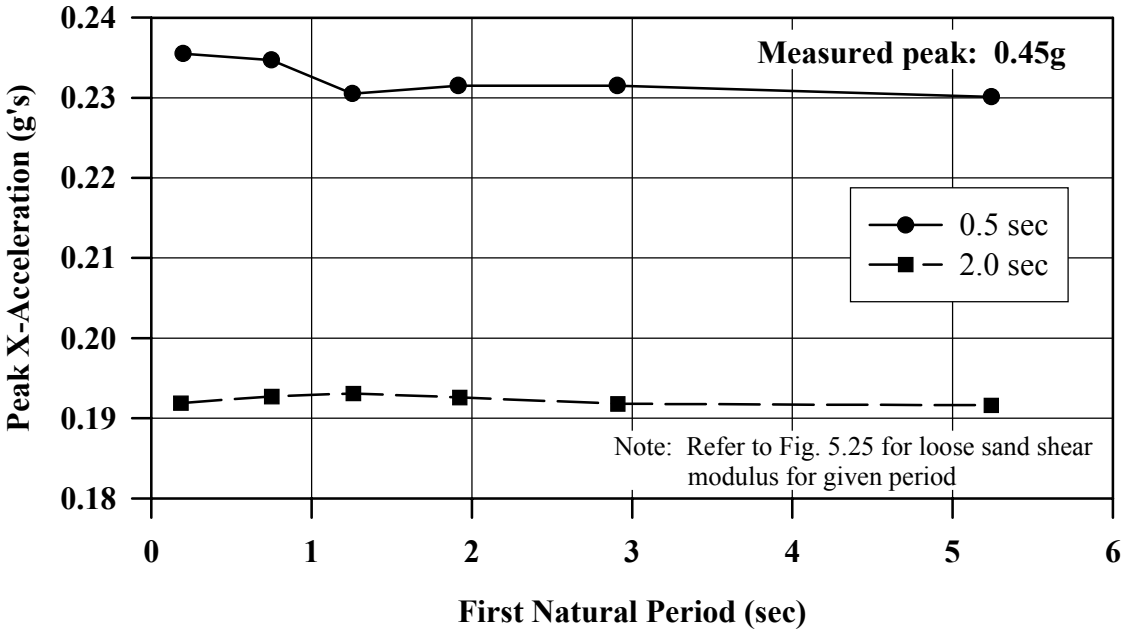

FIGURE 5.28: Variation of Predicted Peak X-Acceleration at CA7 in Dense Zone with System Period for Different Input Motion Periods

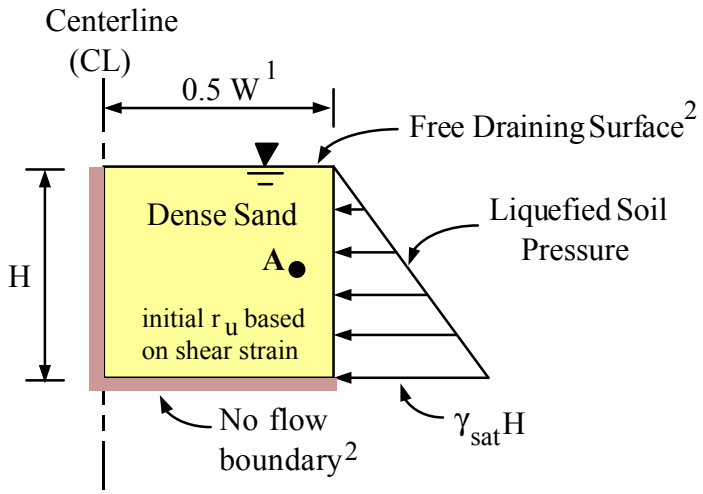

(a) Migration Phase [3]

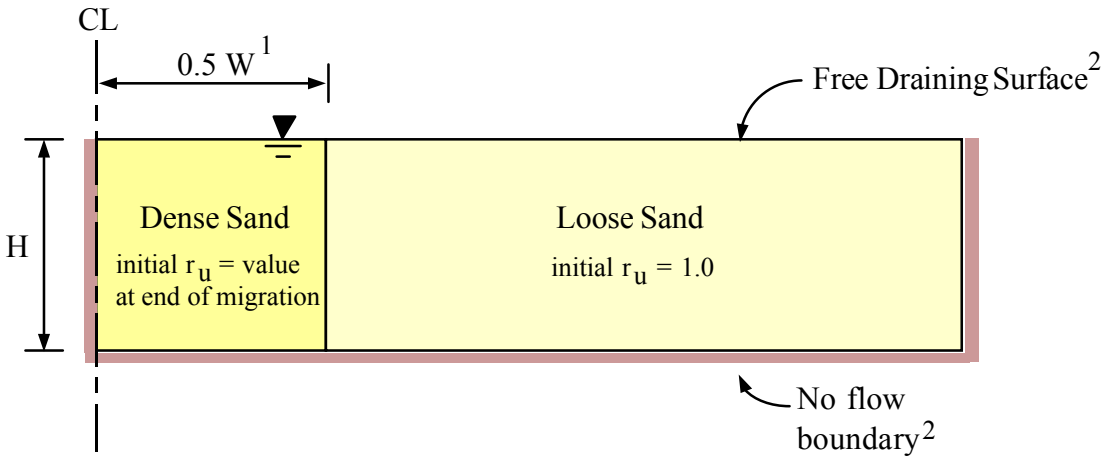

(b) Dissipation Phase [3]

Notes:
1. W is full width of treatment zone. Using symmetry only one-half of full width is modelled.
2. Boundary condition which is problem specific.
3. Properties and dimensions used for analysis giving excess pore pressure ratio at Point A (located 5.5 m from bottom and 10 m from centerline) plotted in Figure 5.30:
   H = 11 m 0.5W = 12 m
   Dense zone - $k = 3 \times 10^{-5}$ m/sec $S_s = 3 \times 10^{-5}$ m^{-1} $\gamma_{sat} = 20.3$ kN/m^3
   Loose zone - $k = 6 \times 10^{-5}$ m/sec $S_s = 1 \times 10^{-4}$ m^{-1} $\gamma_{sat} = 19.0$ kN/m^3
   where k = hydraulic conductivity and S_s = Specific storage = $m_v \gamma_w$

FIGURE 5.29: Combined Migration and Dissipation Analysis

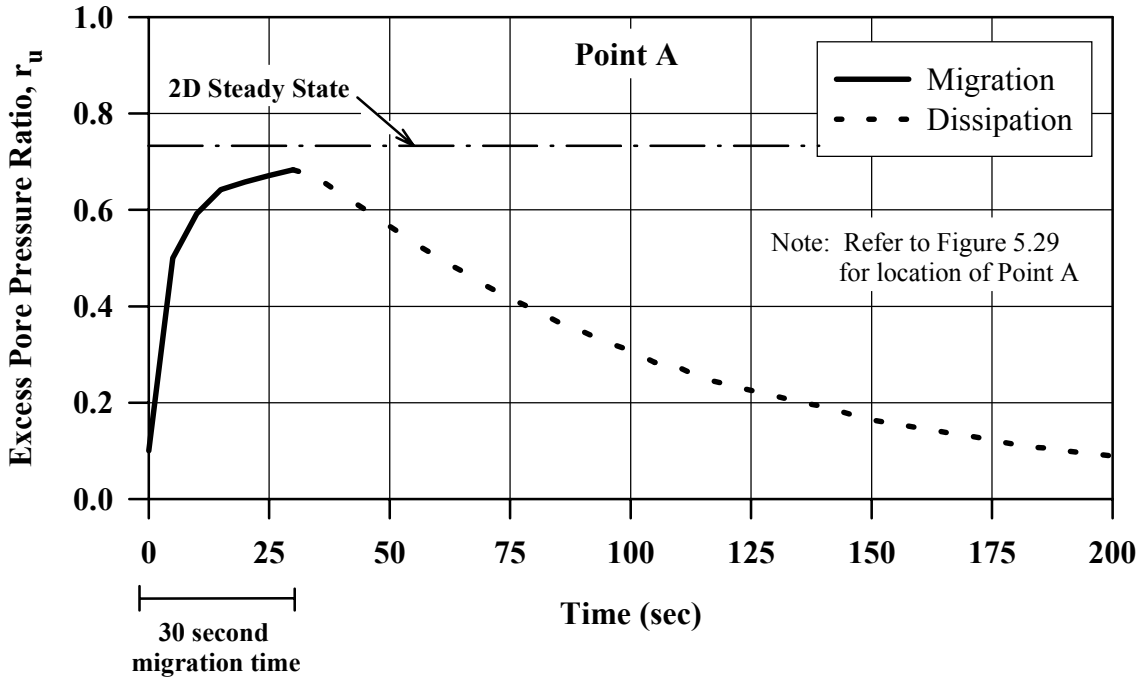

FIGURE 5.30: Example of Excess Pore Pressure Ratio vs. Time Plot for Point A in Dense Sand from 2D Combined Migration and Dissipation Analysis (after Schaeffer, 1998)

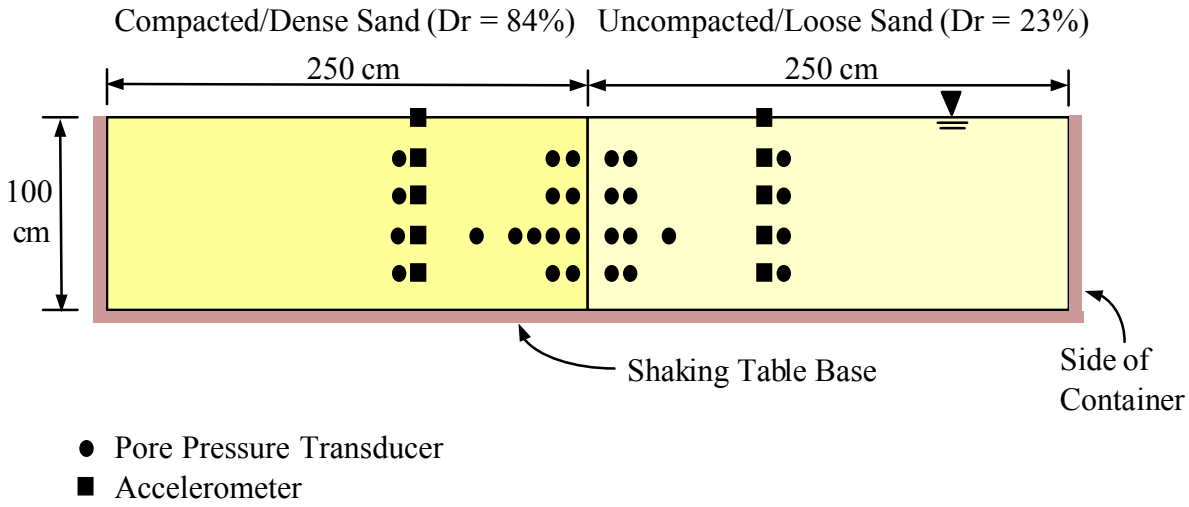

FIGURE 5.31: Cross-section of Shaking Table Test by Iai et al. (after Iai et al., 1988)

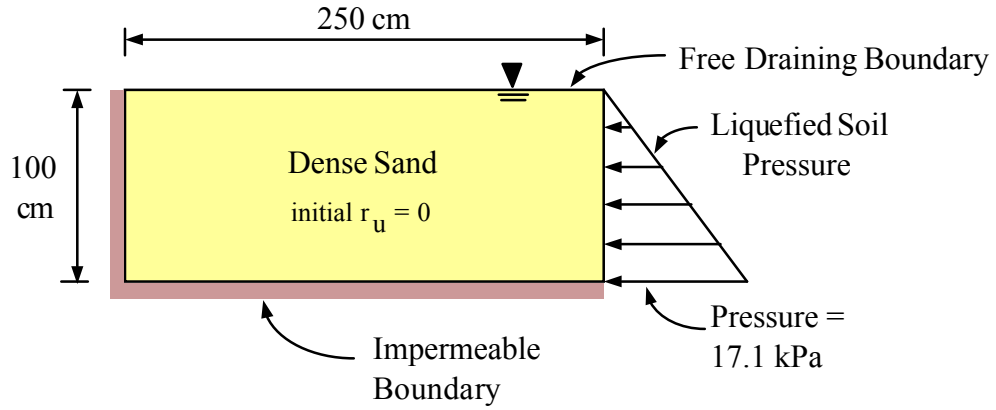

(a) Migration Phase

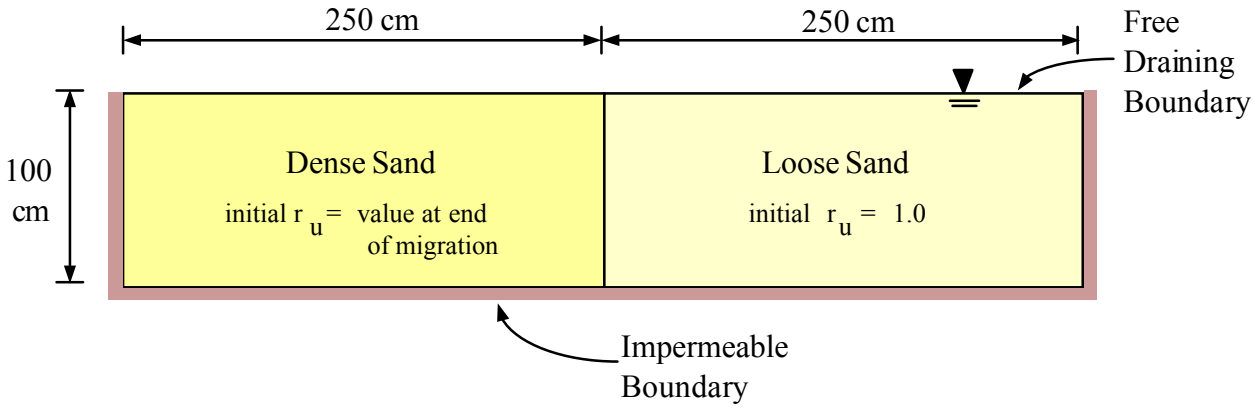

(b) Dissipation Phase

FIGURE 5.32: Migration and Dissipation Analyses of Shaking Table Tests by Iai et al. (after Schaeffer, 1998)

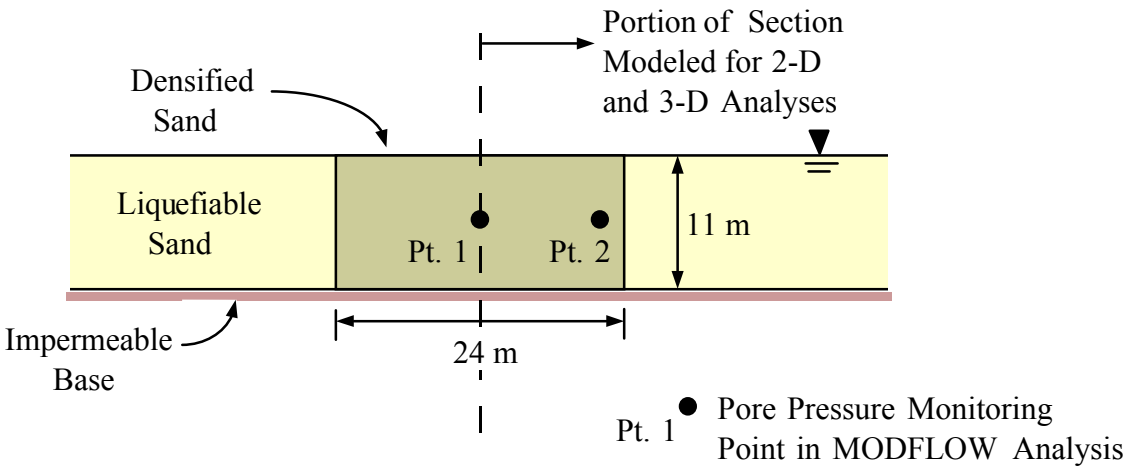

(a) Section

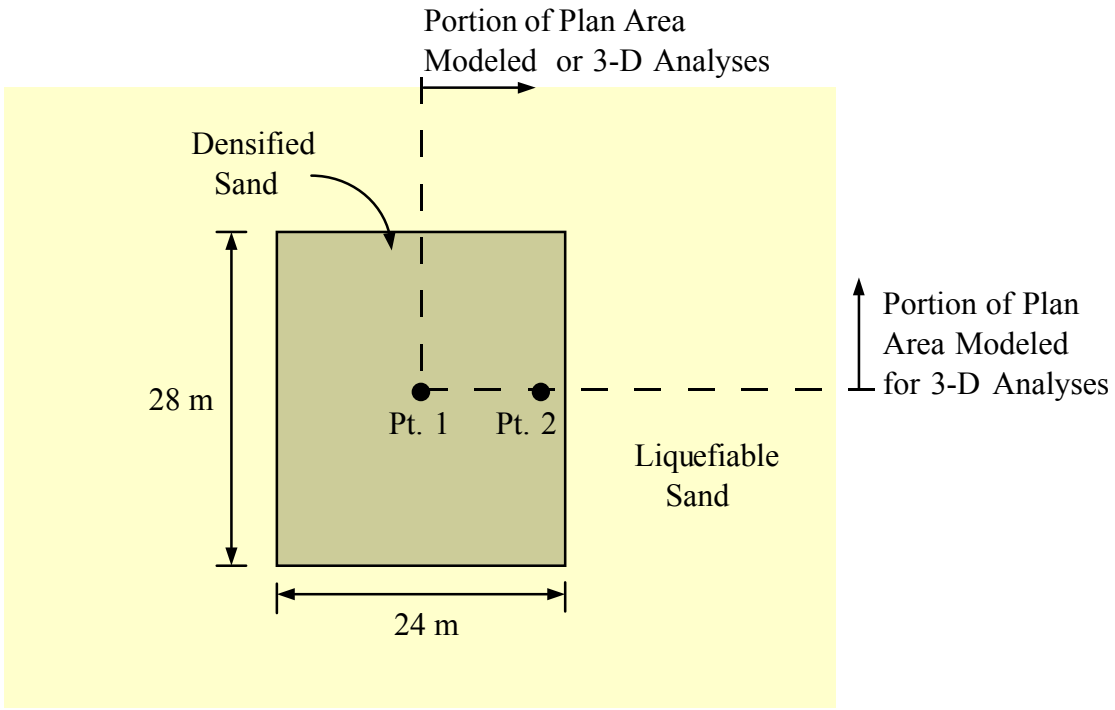

(b) Plan View

FIGURE 5.33: Densified Zone Configuration Used in Study of Pore Pressure Migration and Dissipation

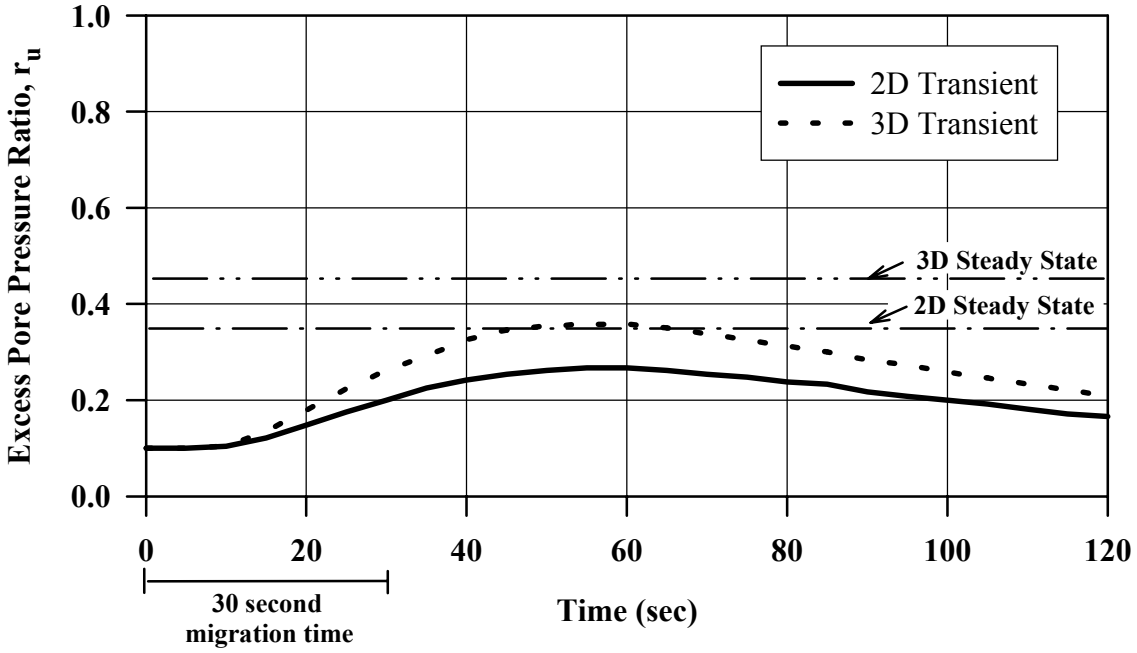

(a) Point 1

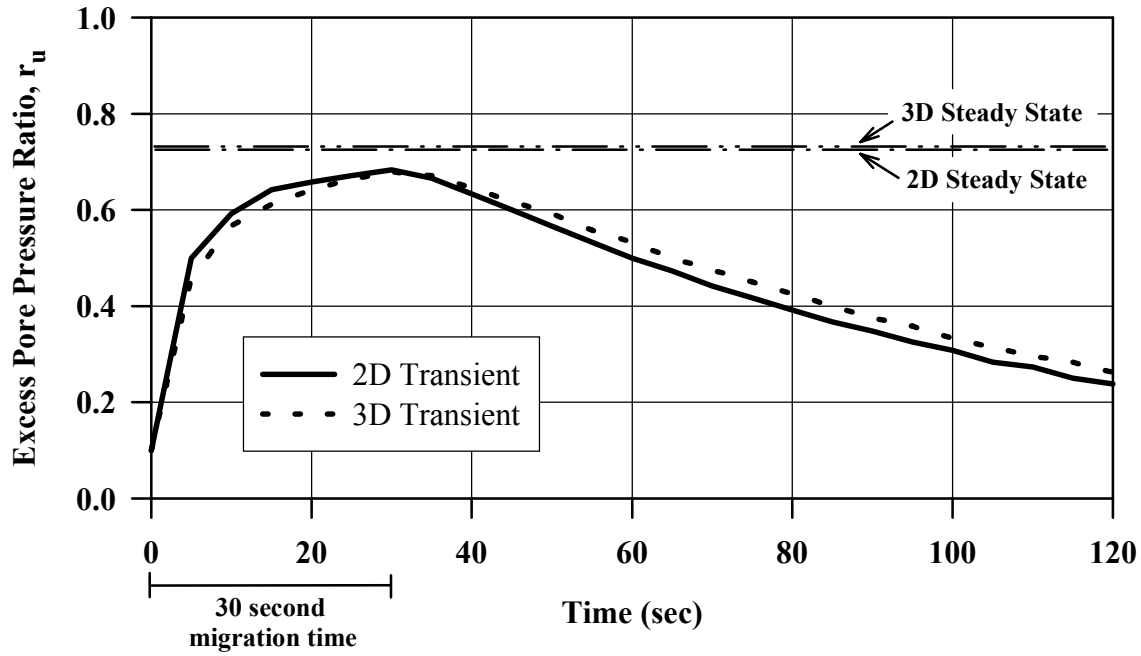

(b) Point 2

FIGURE 5.34: Predicted Excess Pore Pressure Ratios at Two Points in Densified Block

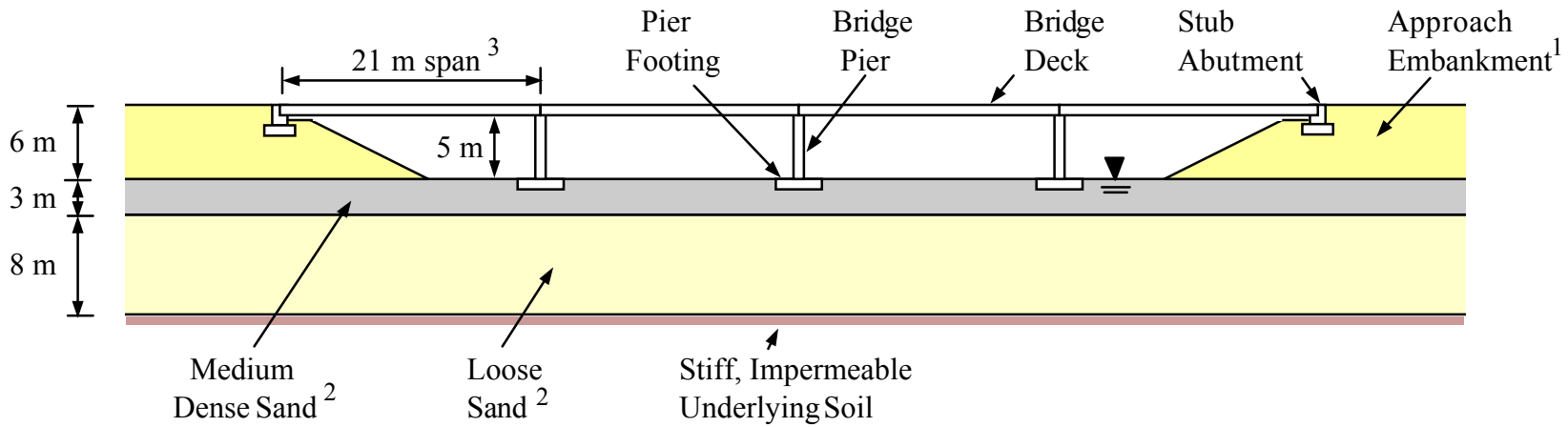

Notes: 1. Approach embankment constructed of dense, well-graded gravelly sand.
2. Gradation of loose and medium dense sands is fine to medium.
3. All bridge spans are 21 m in length and support 8 m wide deck.

FIGURE 5.35: Elevation View of Bridge Used for Test Problem

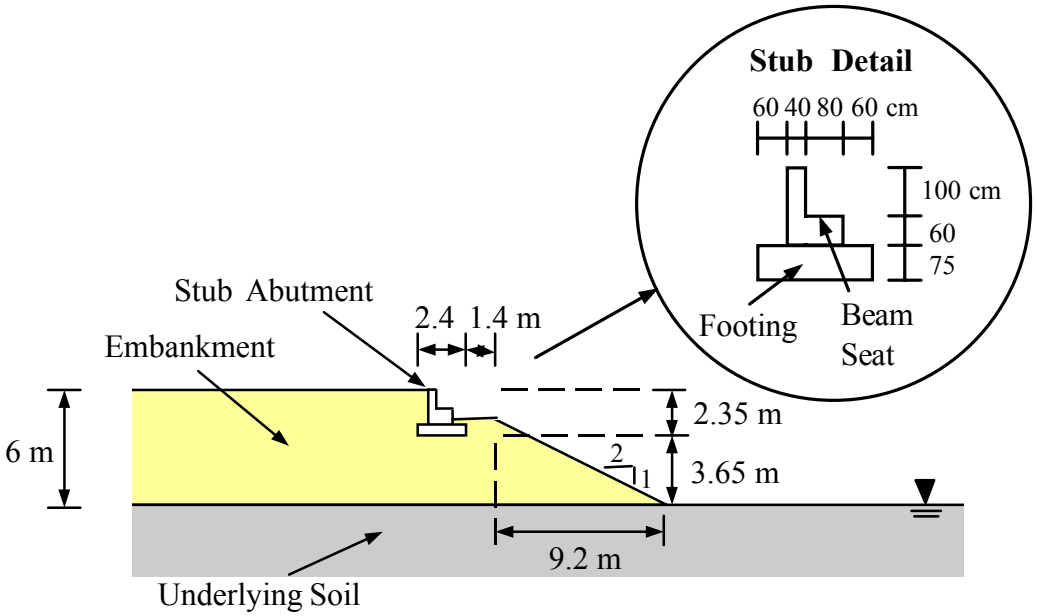

(a) Elevation View

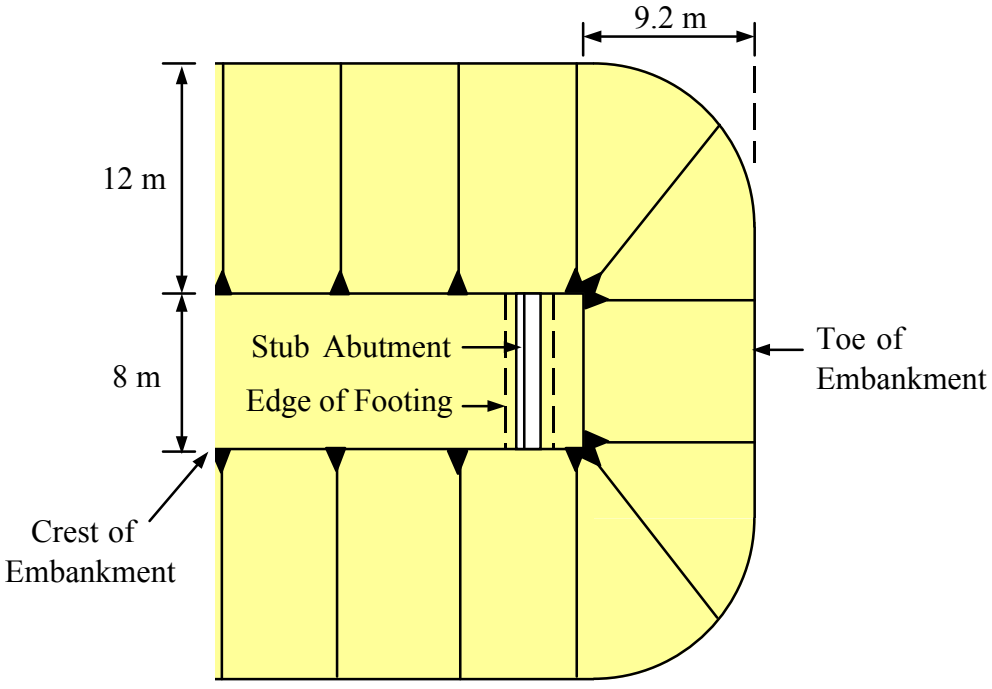

(b) Plan View

FIGURE 5.36: Plan and Elevation Views of Bridge Stub Abutment for Test Problem

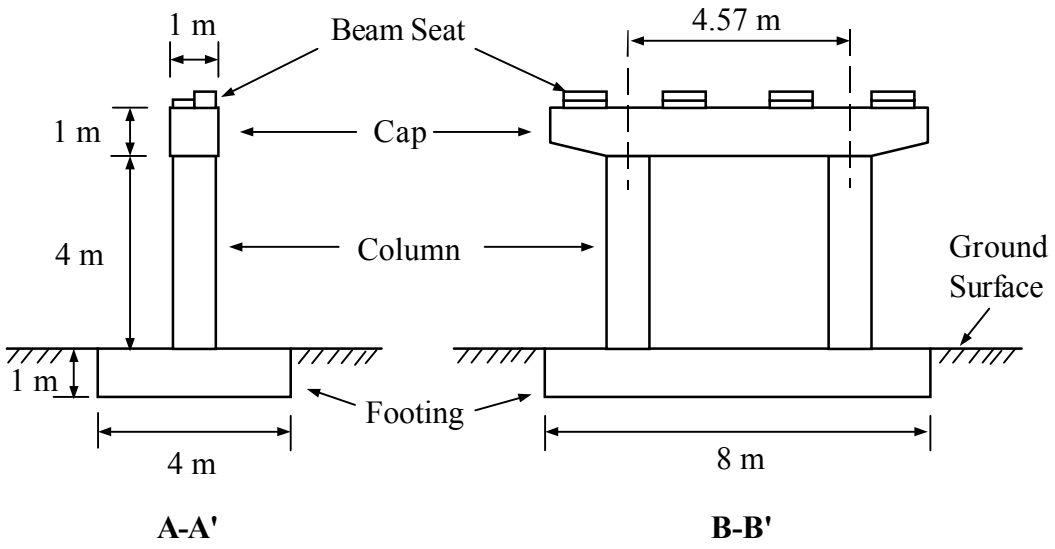

(a) Sections

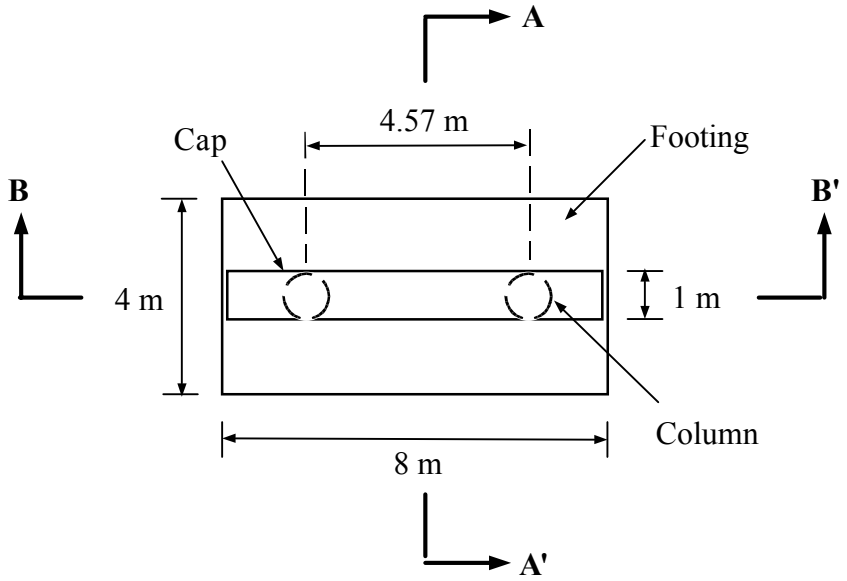

(b) Plan View

FIGURE 5.37: Plan and Section Views of Bridge Pier for Test Problem

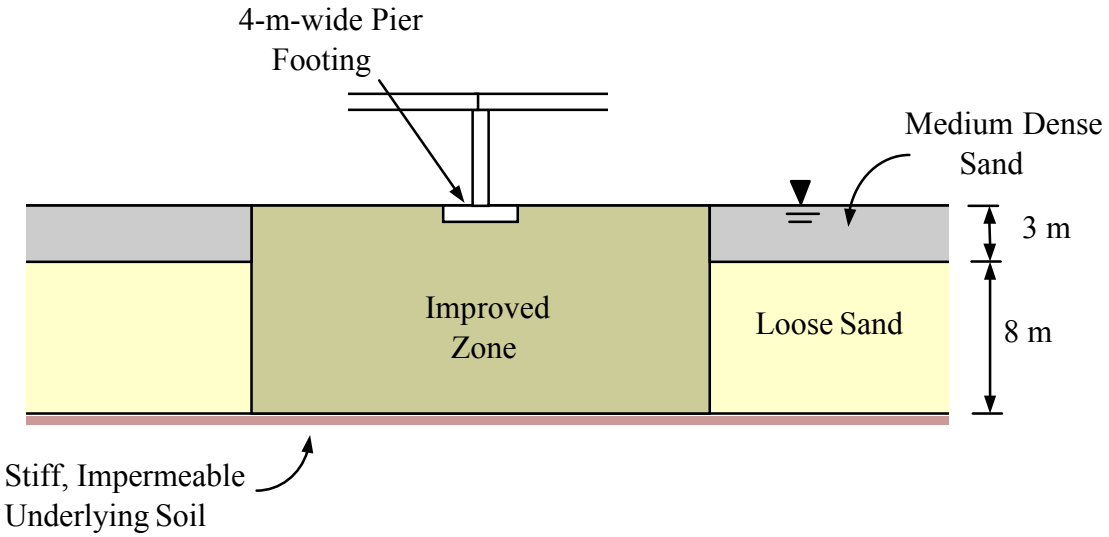

(a) Elevation View

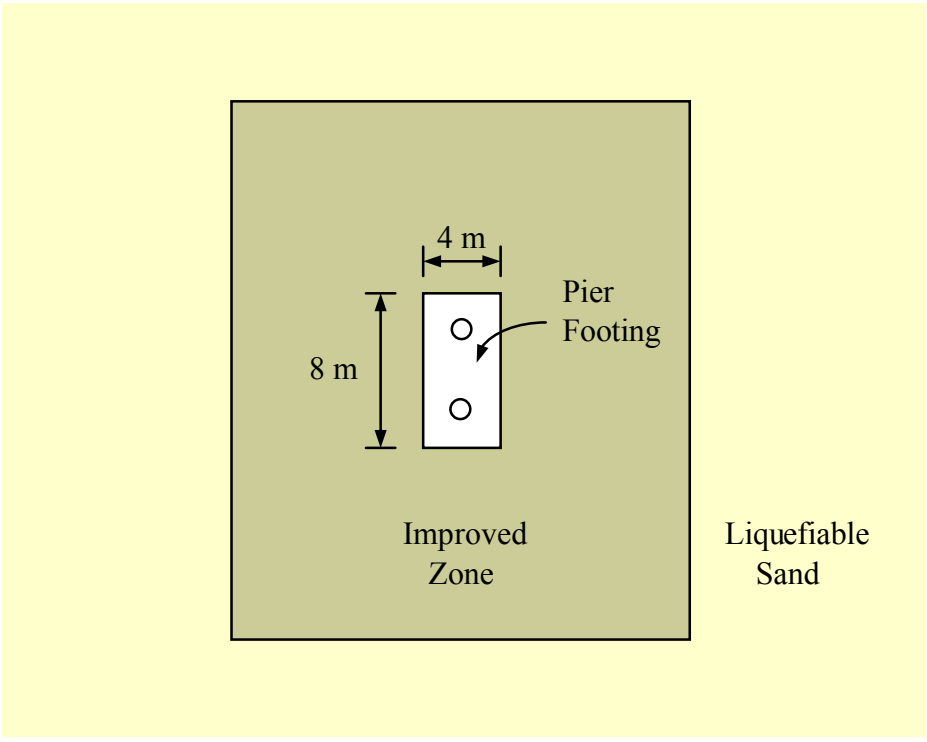

(b) Plan View

FIGURE 5.38: Improved Ground Zone Used at Bridge Pier

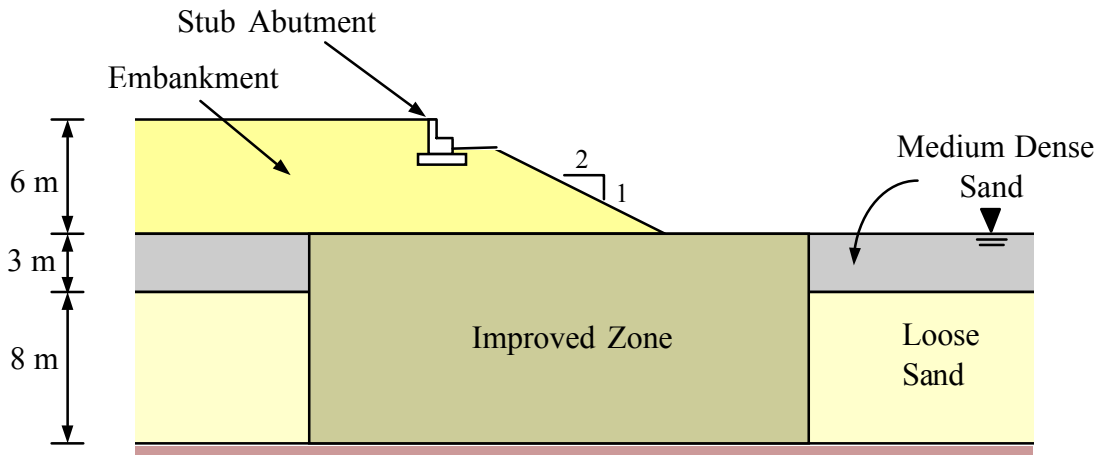

(a) Elevation View

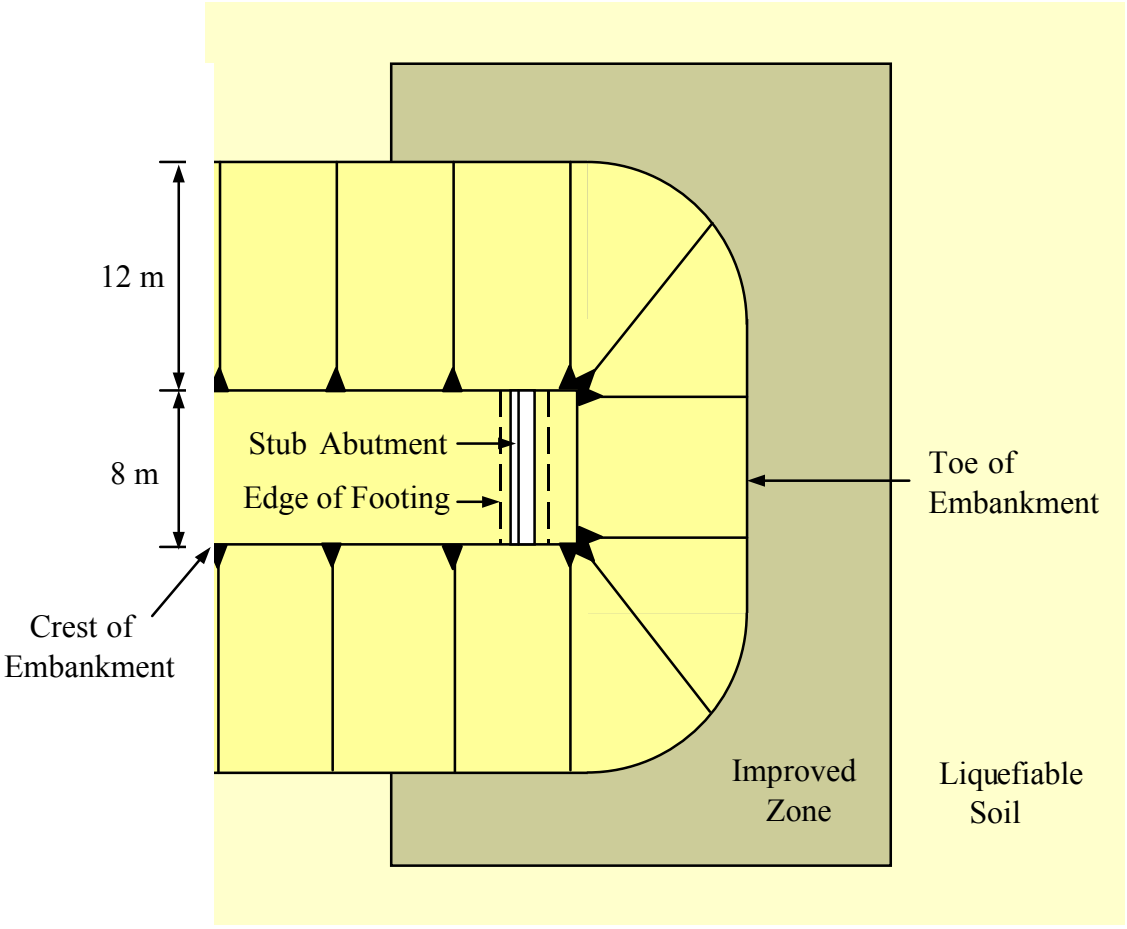

(b) Plan View

FIGURE 5.39: Improved Zone at Bridge Stub Abutment

Pressures:
x = 20 kPa over 3 m at 11 degrees from vertical[1]
y = 24 kPa over 1.9 m at 11 degrees from vertical
z = 156 kPa over 2.1 m at 15 degrees from vertical
y and z are pressures over bottom of pier footing

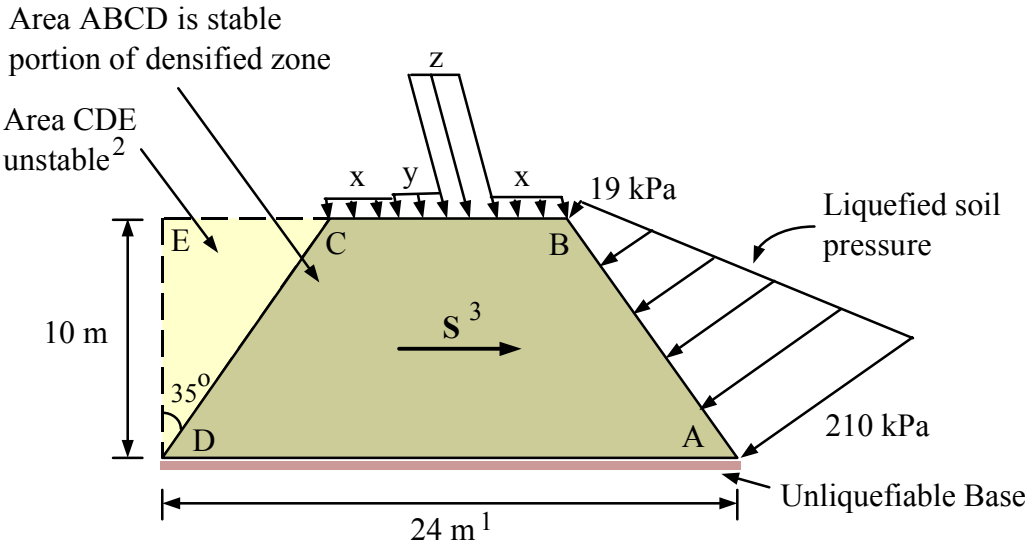

Notes: 1. Widths of 19 m and 34 m were also evaluated. For these cases x acts on each side of footing over widths of 0.5 m and 8 m, respectively.
2. Unstable area, like CDE, also exists on right side of densified zone. These areas replaced by liquefied soil pressure distribution, like one shown along line AB.
3. S is seismic coefficient which is equal to the ratio of assumed horizontal acceleration induced by earthquake in soil mass divided by downward gravitational acceleration.

FIGURE 5.40: Configuration for Pseudostatic Stability Analysis of Bridge Pier Footing

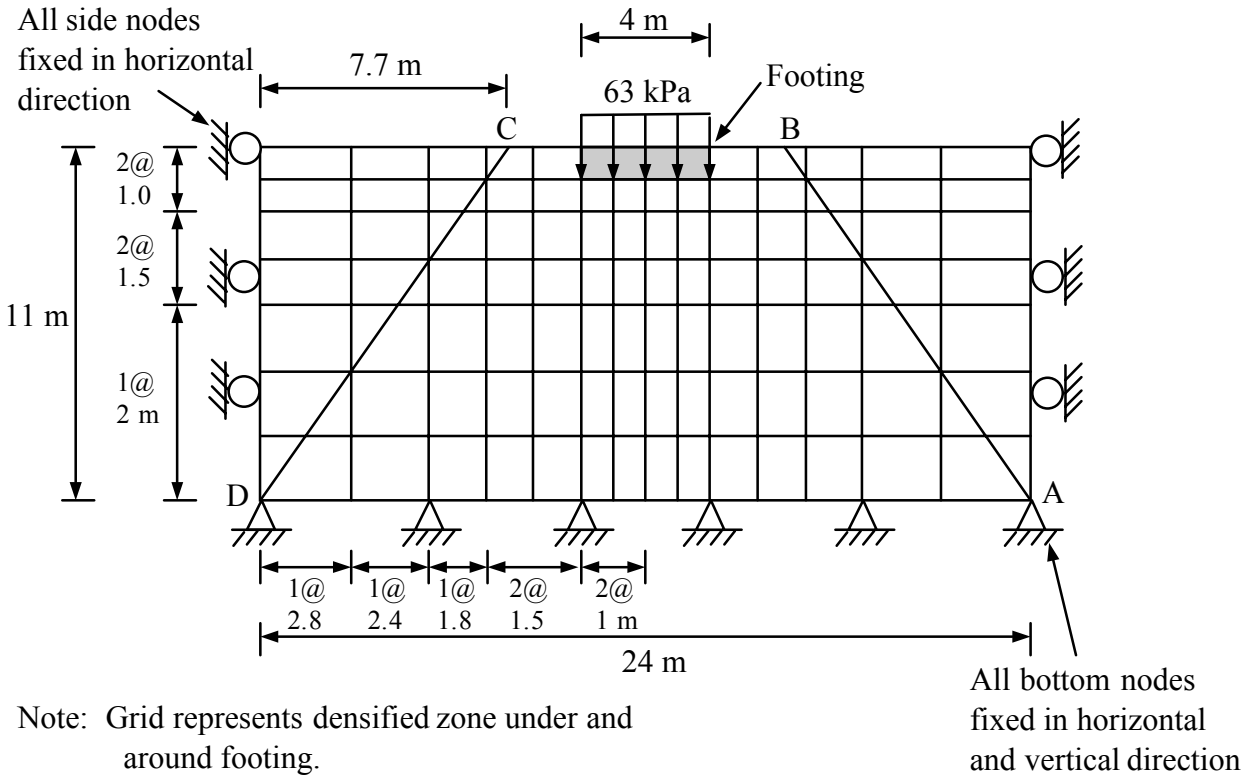

Note: Grid represents densified zone under and around footing.

(a) Pre-earthquake Conditions

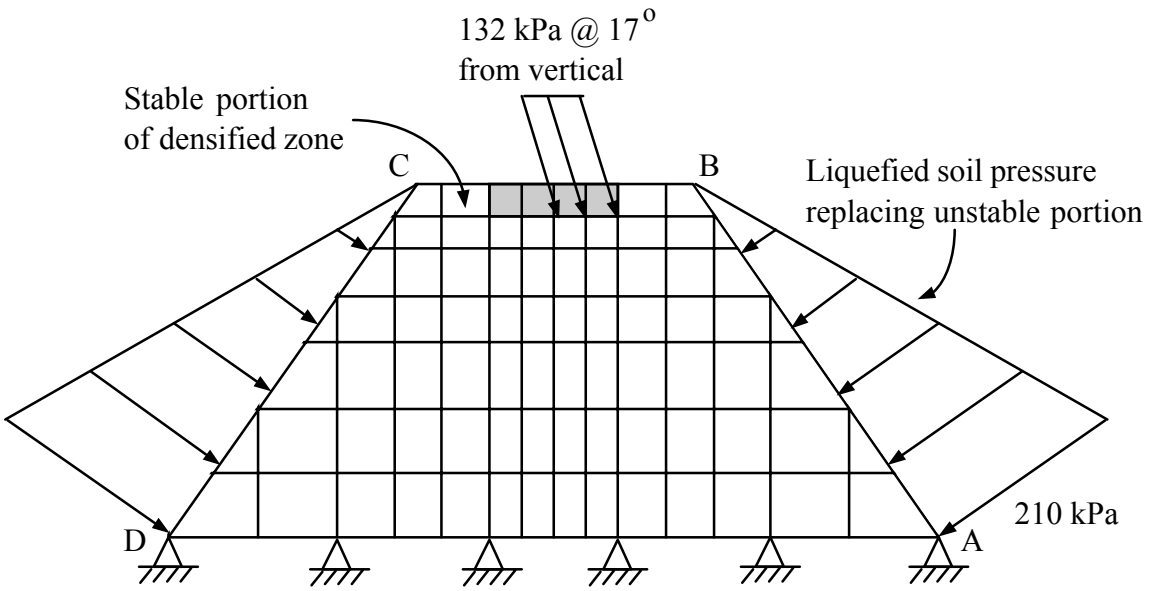

Note: Seismic coefficient included in analysis imposing body forces acting towards right side to represent inertial effects on soil.

(b) Earthquake Conditions

FIGURE 5.41: Finite Element Mesh and Boundary Conditions Used in Pseudostatic Deformation Analyses for Densification to 10 meter Outside Footing

Pressures:
x = 20 kPa over 3 m at 11 degrees from vertical
y = 24 kPa over 1.9 m at 11 degrees from vertical
z = 156 kPa over 2.1 m at 15 degrees from vertical
y and z are pressures over bottom of pier footing

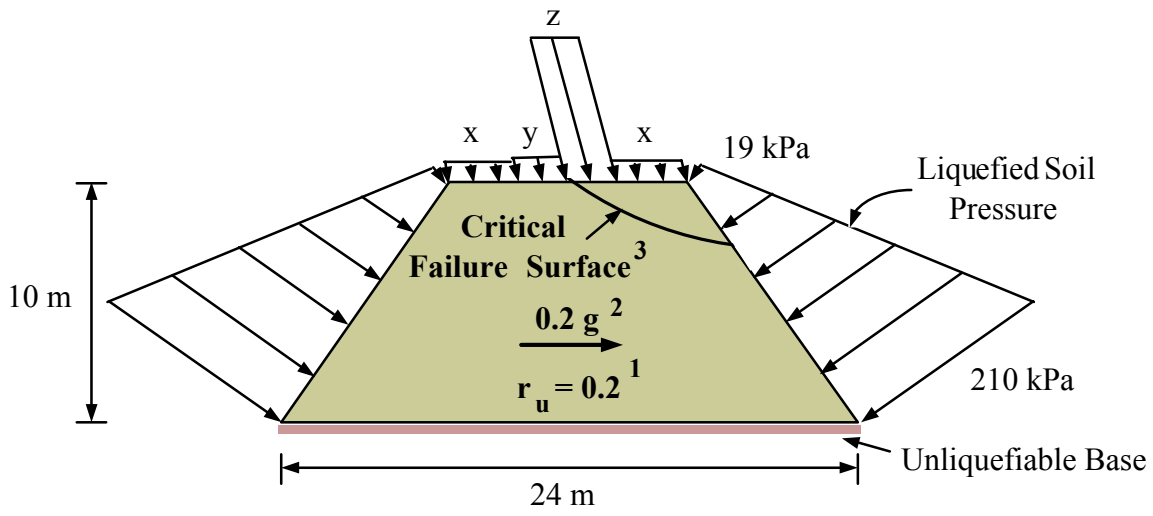

Notes: 1. Excess pore water pressure ratio, r_u, of 0.2 assumed in analysis.
2. Seismic coefficient of 0.2 assumed in analysis.
3. Critical failure surface has calculated safety factor of 1.06 by Spencer's method.

FIGURE 5.42: Example of Critical Failure Surface for Pseudostatic Stability Analysis of Bridge Pier Footing

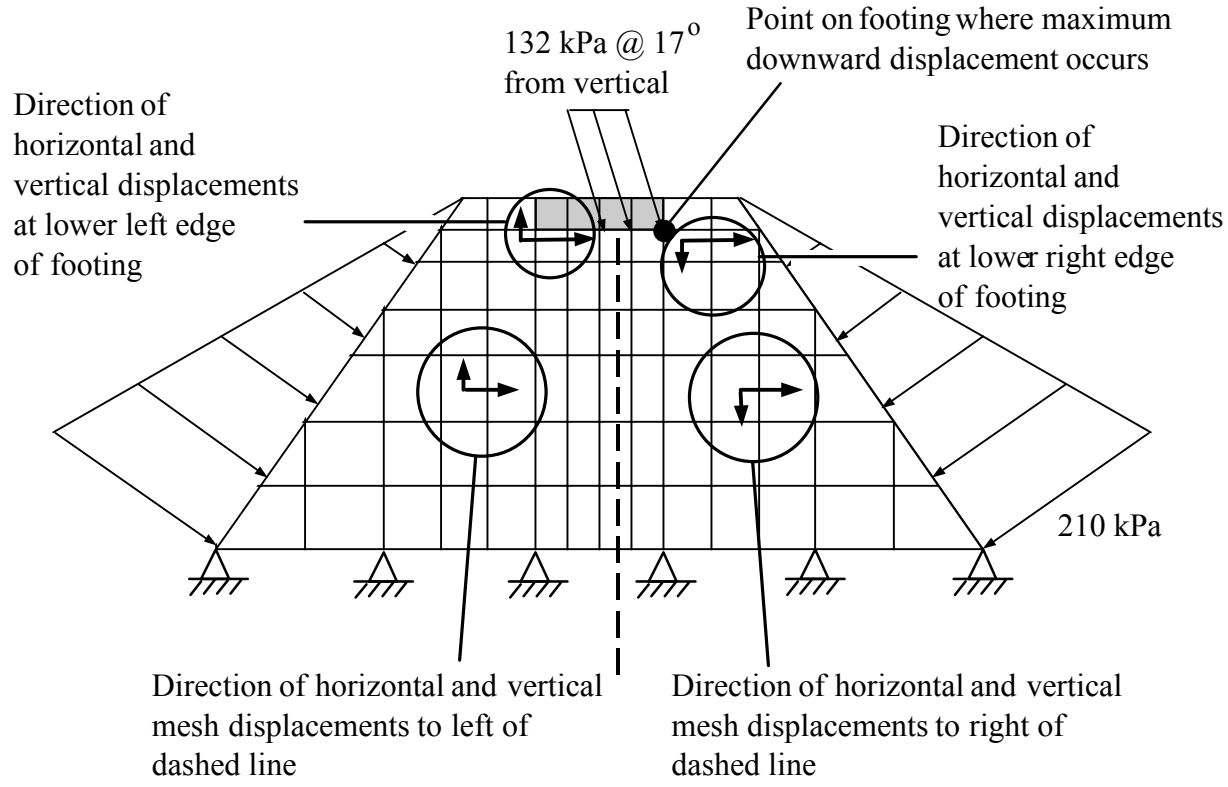

Note: Seismic coefficient included in analysis imposing body forces acting towards right side to represent inertial effects on soil.

FIGURE 5.43: Typical Direction of Displacements Observed in Pseudostatic Deformation Analyses

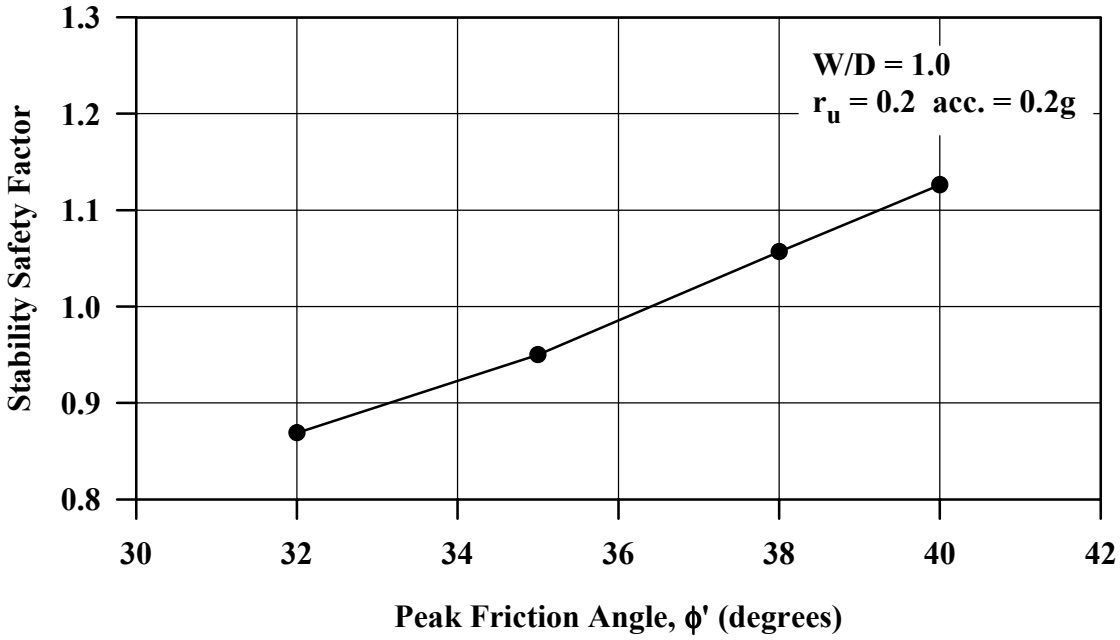

FIGURE 5.44: Effect of Soil Strength on Stability Safety Factor for Pier Footing on Densified Zone

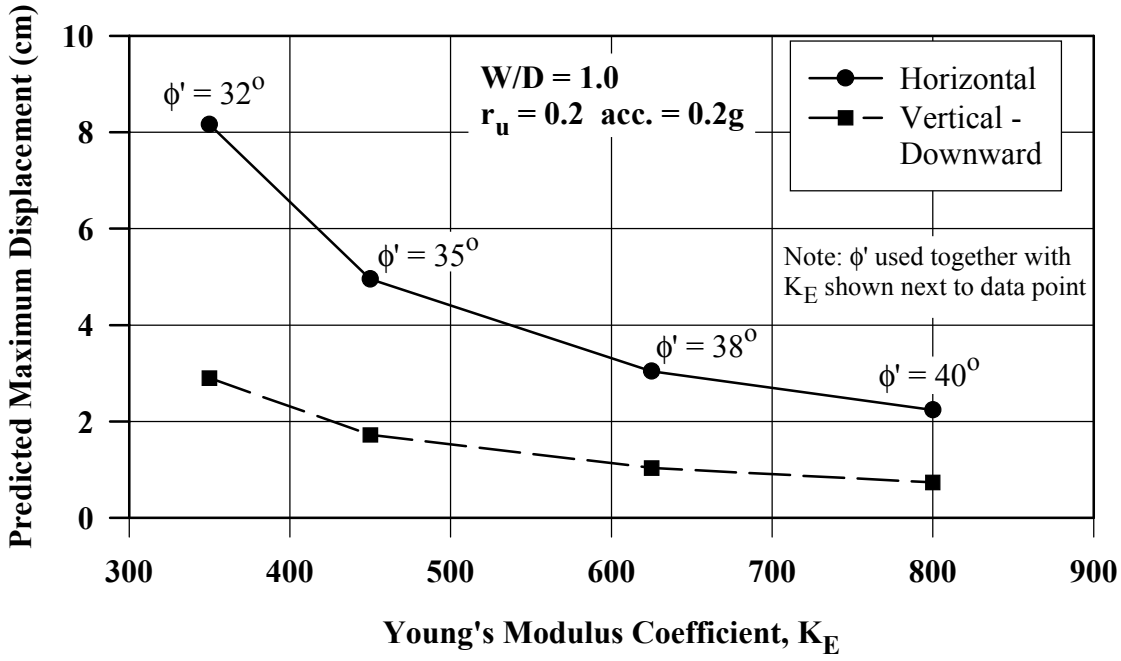

FIGURE 5.45: Effect of Soil Stiffness on Predicted Maximum Displacements of Pier Footing on Densified Zone

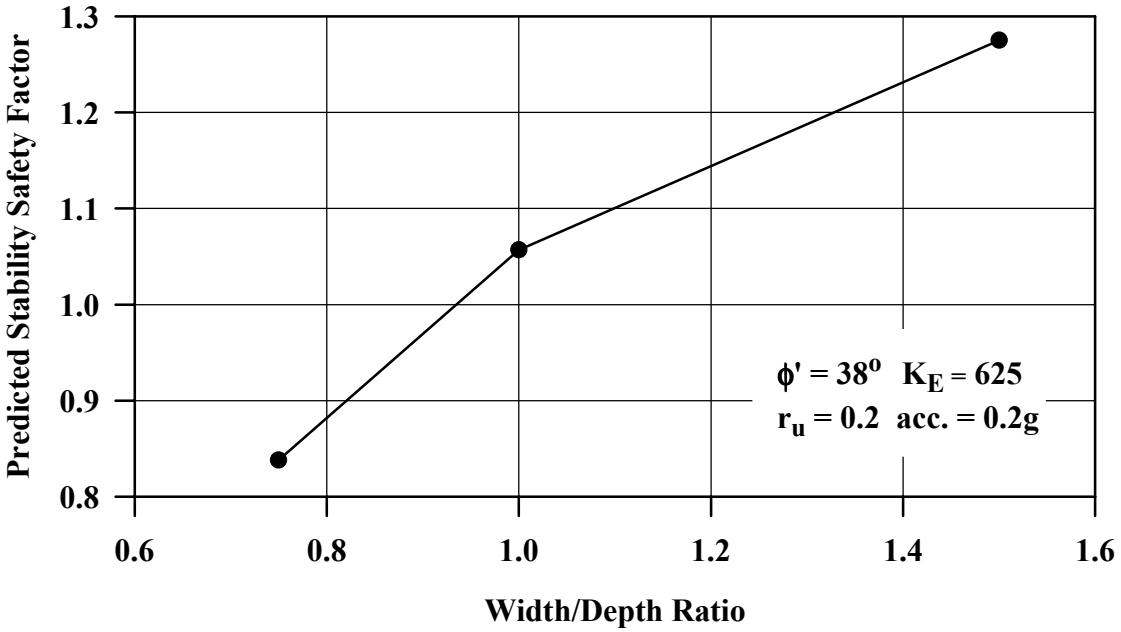

FIGURE 5.46: Effect of Width/Depth Ratio of Dense Zone on Predicted Stability Safety Factor for Pier Footing

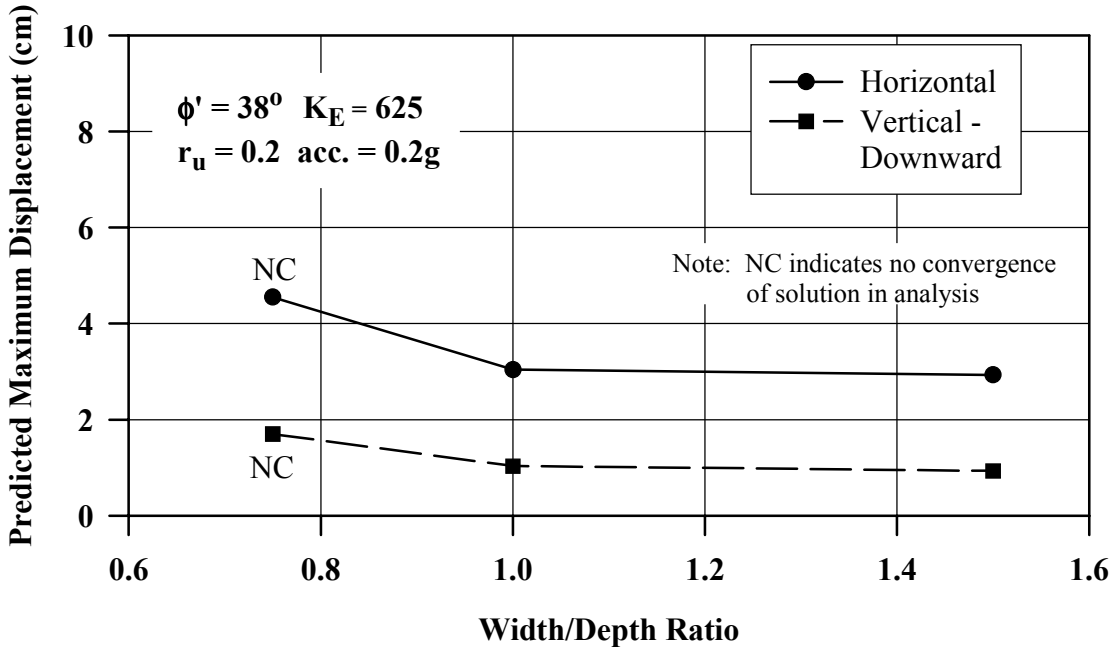

FIGURE 5.47: Effect of Width/Depth Ratio of Dense Zone on Predicted Maximum Displacements of Pier Footing

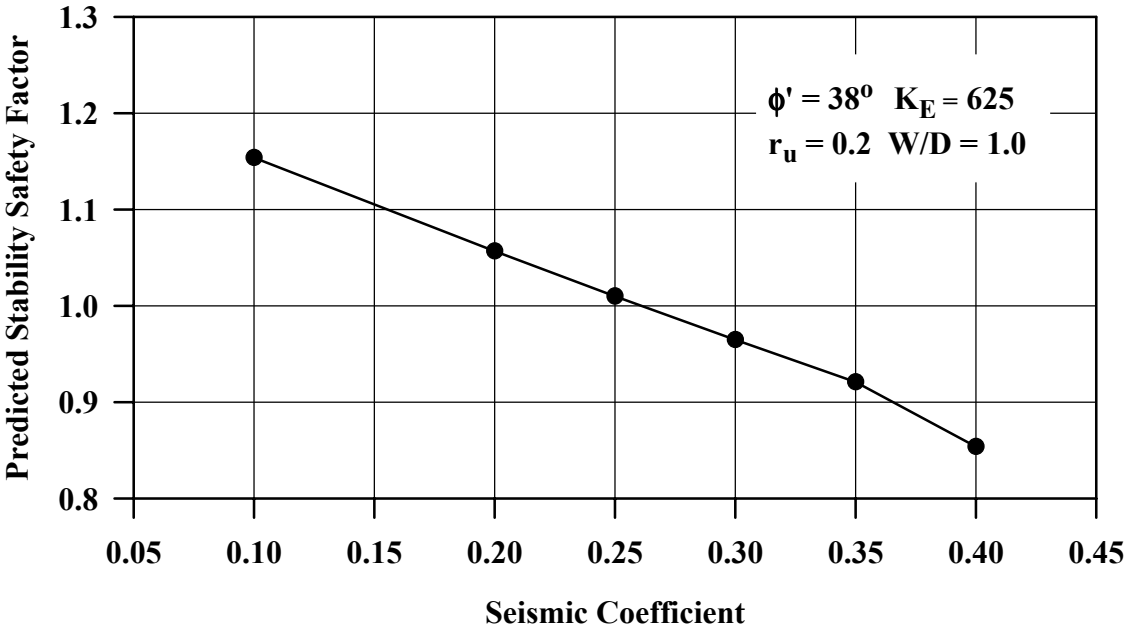

FIGURE 5.48: Effect of Seismic Coefficient on Predicted Stability Safety Factor for Pier Footing on Densified Zone

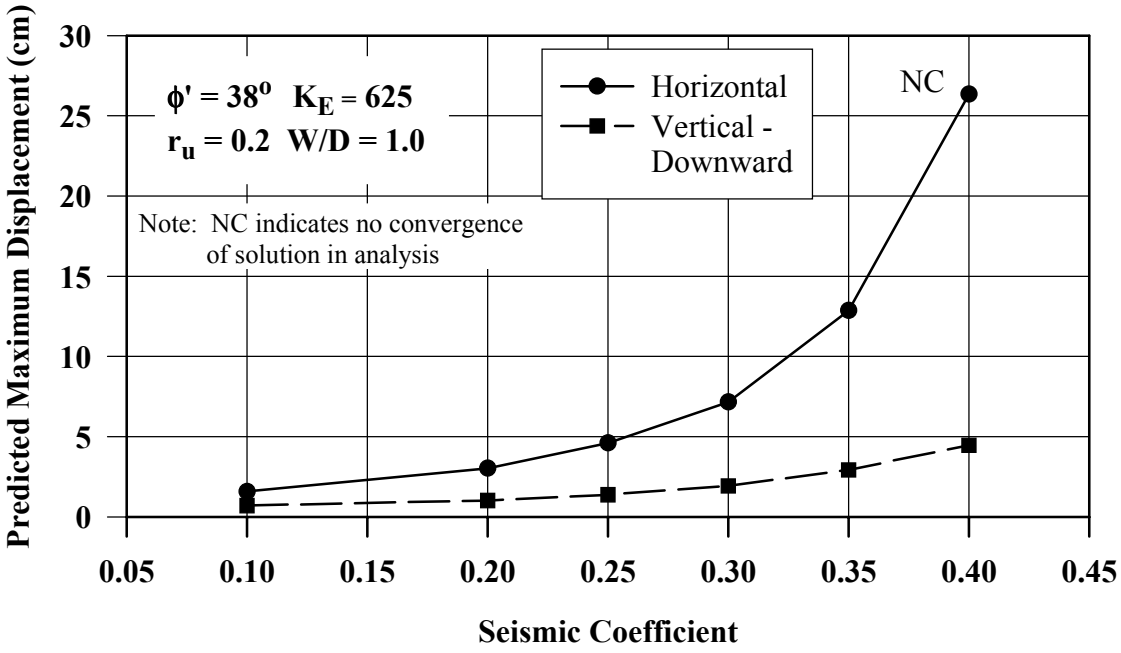

FIGURE 5.49: Effect of Seismic Coefficient on Predicted Maximum Displacements of Pier Footing on Densified Zone

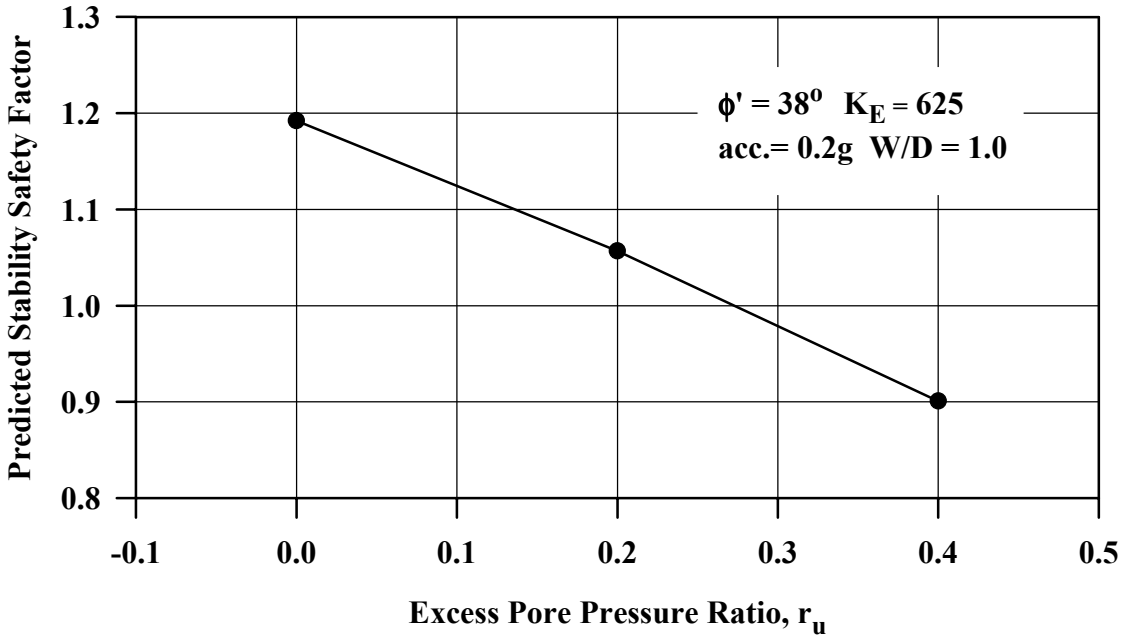

FIGURE 5.50: Effect of Excess Pore Pressure Ratio in Dense Zone on Predicted Stability Safety Factor for Pier Footing

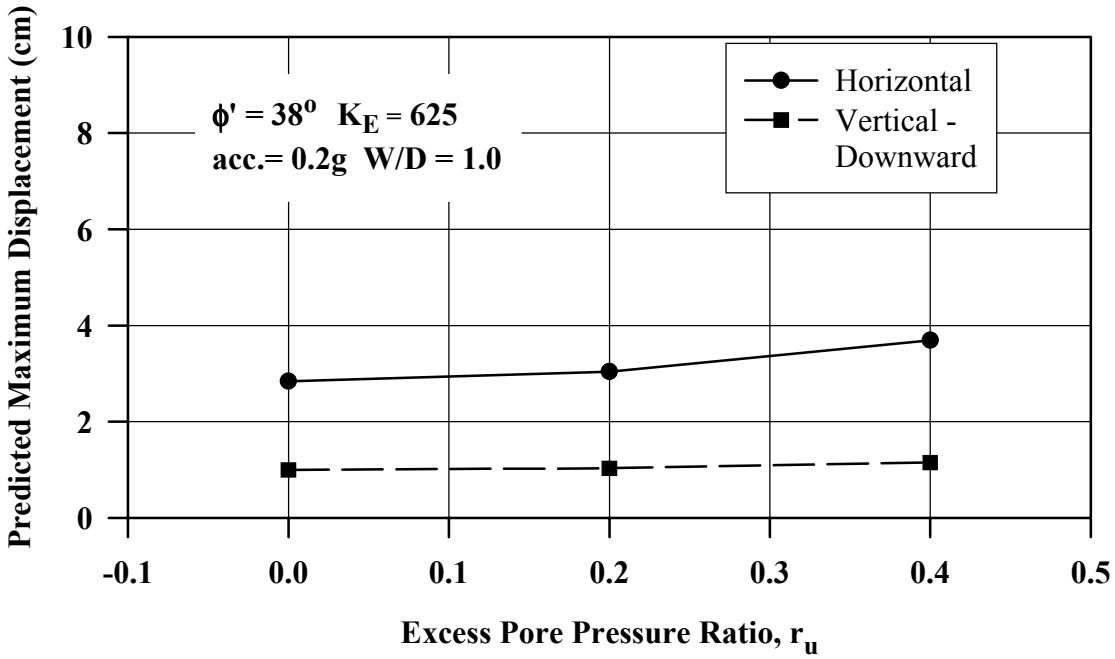

FIGURE 5.51: Effect of Excess Pore Pressure Ratio in Dense Zone on Predicted Maximum Displacements of Pier Footing